Dissertations, Master's Theses and Master's Reports

2017

CONTINUOUS HYDROLOGIC MODELING FOR ANALYZING THE EFFECTS OF DROUGHT ON THE LOWER COLORADO RIVER IN TEXAS

Khalid Samady
Michigan Technological University, mksamady@mtu.edu

CONTINUOUS HYDROLOGIC MODELING FOR ANALYZING THE EFFECTS OF

DROUGHT ON THE LOWER COLORADO RIVER IN TEXAS.

By

Mohammad Khalid Samady

A THESIS

Submitted in partial fulfillment of the requirements for the degree of

MASTER OF SCIENCE

In Civil Engineering

MICHIGAN TECHNOLOGICAL UNIVERSITY

2017

This thesis has been approved in partial fulfillment of the requirements for the Degree of MASTER OF SCIENCE in Civil Engineering.

Department of Civil and Environmental Engineering

Thesis Advisor: *Dr. David W. Watkins, Jr.*

Committee Member: *Dr. Brian D. Barkdoll*

Committee Member: *Mike D. Hyslop*

Department Chair: *Dr. Audra N. Morse*

To all Afghan kids who are the bright future of the country.

Contents

List of figures

List of tables

Acknowledgements

I would like to present my sincere gratitude to my thesis advisor Dr. David W. Watkins, for his personal and professional guidance. I am grateful for knowing such a knowledgeable, patient, humble and helpful mentor in my life.

Besides my advisor, I would like to acknowledge my thesis committee, Dr. Brian Barkdoll. As my teacher in river hydraulics, stream restoration, low impact development and stormwater management courses, he has taught me more than I could ever give him credit. I also acknowledge Mr. Mike Hyslop, who taught me the basics of geographical information system, which I used to develop my model. I would also acknowledge my adviser and committees for their insightful comments and encouragement, as well as review of this thesis.

I am grateful to the U.S. Department of State, The Fulbright team, and the Michigan Tech Graduate School for supporting and sponsoring my education.

I would like to thank my family: my parents and to my brothers and sister for encouraging, motivating and supporting me through my life.

And I thank Allah for all his blessings upon me.

Abstract

A physically based hydrologic model, the HEC-Hydrologic Modeling System (HMS), developed by the U.S. Army Corps of Engineers, has been parameterized using the Soil Moisture Accounting (SMA) algorithm, calibrated, and validated for the Lake Travis and Lake Lyndon B. Johnson (LBJ) contributing basins in central Texas. The basins are divided into a total of 15 sub-basins, and HEC-HMS with the SMA algorithm represents each sub-basin with five water storage layers involving twelve parameters-- surface depression storage, canopy interception storage, upper zone soil storage, tension zone soil storage, infiltration rate, and soil percolation rate, along with storage depths, storage coefficients and percolation rates for one shallow and one deep groundwater layer. The first six parameters and the percolation rate for the interflow were estimated objectively using a combination of the National Land Cover Database 2011 (NLCD 2011) and Soil Survey Geographic Database (SSURGO). The next four parameters were estimated based on analysis of historical streamflow records, and the last parameter was determined through model calibration. The parameter analysis shows that the tension zone storage, interflow storage coefficient and the baseflow percolation rate are the most sensitive parameters for this watershed model.

Comparison of simulated and observed streamflows showed that the estimated parameters can be used with meteorological data to simulate flows into the Highland Lakes system in central Texas. The results of the statistical analysis indicate that the simulated flows and observed flows are reasonably well correlated. The model performance is rated as good to very good for all the metrics. The PBIAS coefficient is 9.6 and the Nash-Sutcliffe efficiency value is 0.71 for the entire simulation period, 2004-2016. The model performance can potentially be improved through further calibration and by using the hourly climatic input data instead of daily data.

In future work, the validated HEC-HMS model can be employed with seasonal climate forecasts and under long-range land-use and climate projections. In addition, radar-based precipitation data can be used to represent the climatic variability on a grid-based scale.

Chapter 1. Introduction

1.1   Problem and Research Objective

Central Texas was afflicted by severe hydrologic drought from 2008 through 2015. The inflows to Lake Travis and Lake Buchanan on the Lower Colorado River were the lowest in 2011 at only about 11 percent of average (LCRA, 2017a-b). Ryu et al. (2014) stated that the 2011 drought cost the state an estimated $7.6 billion dollars in economic losses affecting local businesses, farmers, and municipalities. Therefore, water managers need to develop a better water management plan to understand the consequences of extreme hydrologic events, and improve forecasts to mitigate effects of droughts in the Lower Colorado River basin.

This paper explains the parameterization process of HEC-HMS with SMA model that can simulate stream flows on a daily time step for the Lake Travis and Lake Buchanan-Lyndon B. Johnson (LBJ) basins in central Texas. Based on the literature review, this study is the first application of a continuous HEC-HMS model with the SMA algorithm using the Penman–Monteith equation combined with the Bristow and Campbell Algorithm and FAO56 solar radiation calculation methods for modeling evapotranspiration. In addition, this model accounts for spatial hydrologic variability in more sub-basins and the analysis of results also focuses on drought impacts.

This thesis is organized into five chapters. The first chapter summarizes research objectives and contains background information about the Lower Colorado River Authority (LCRA) and Highland Lakes watershed characteristics. Chapter 2 provides an overview of hydrological models, including related studies, and. Chapter 3 describe HEC-HMS model setup and SMA parameterization. The next chapter discusses the calibration process and model results, and the final chapter presents conclusions, limitations, and future work.

1.2 Background

1.2.1 Colorado River

The Colorado River is 862 miles long, making it the largest river, by length and drainage area, within the state of Texas (Clay et al., 2017). The River originates south of Lubbock, on the Llano Estacado. Its drainage area is more than 42,000 square miles (LCRA, 2017a-a), about 16 percent of the total area of Texas, and its average annual runoff reaches a volume of more than 2 million acre-feet near the Gulf of Mexico (Williams et al., 2017). Prior to the construction of dams in the 1930s and 1940s, the residents of central Texas regularly faced extreme events such as drought and flooding. Due to the arid climate, the Colorado River can drop to a trickle during dry and hot weather; however, in the Hill County portion of the basin devastating floods have also caused major problems for the local residents in the area. The Colorado River is managed by three agencies established by the state legislature--the Lower, Central, and Upper Colorado River authorities (Williams et al., 2017).

1.2.2 Lower Colorado River Authority (LCRA)

The Lower Colorado River Authority (LCRA) is a nonprofit public service organization formed through the LCRA Act, passed by the Texas Legislature in November 1934 (LCRA, 2015). The newly formed LCRA managed the water for only ten counties, from the City of San Saba in Central Texas to Matagorda on the Gulf Coast (LCRA, 2017a-a). Today, the LCRA serves 80 counties (Witham, 2015), and the agency's activities are briefly described below.

- **Water**: The LCRA manages the Highland Lakes and Colorado River as a system to supply water for more than 1.1 million people in over 55 Counties (LCRA, 2015). LCRA operates six hydroelectric dams along the Colorado River, Buchanan Dam, Inks Dam, Wirtz Dam, Max Starcke, Mansfield Dam and Tom

Miller Dam. Through these dams, LCRA manages floodwaters and generates hydroelectric power.

- **Environment**: Environmental protection and leadership is an important part of LCRA's mission. The LCRA provides safe drinking water for over a million people, manages public lands, protects natural resources, and supports sustainable economic and community development.

- **Energy**: The LCRA has been the primary wholesale provider of electricity in Central Texas since 1937, currently maintaining a diverse power generation portfolio from different sources such as coal, natural gas, water, and the wind. The LCRA Transmission Services Corporation (TSC) owns more than 300 substations and supports the electric transmission network across the state (Williams et al., 2017)

- **Public Service**: The LCRA provides a variety of public utilities in the area, and it owns more than 40 public parks (about 11,000 acres of parkland), recreation areas and river access sites along the Highland Lakes and lower Colorado River. Through community service programs, the LCRA aims to improve the lives of Texans and foster the conservation of the Colorado River basin's natural resources.
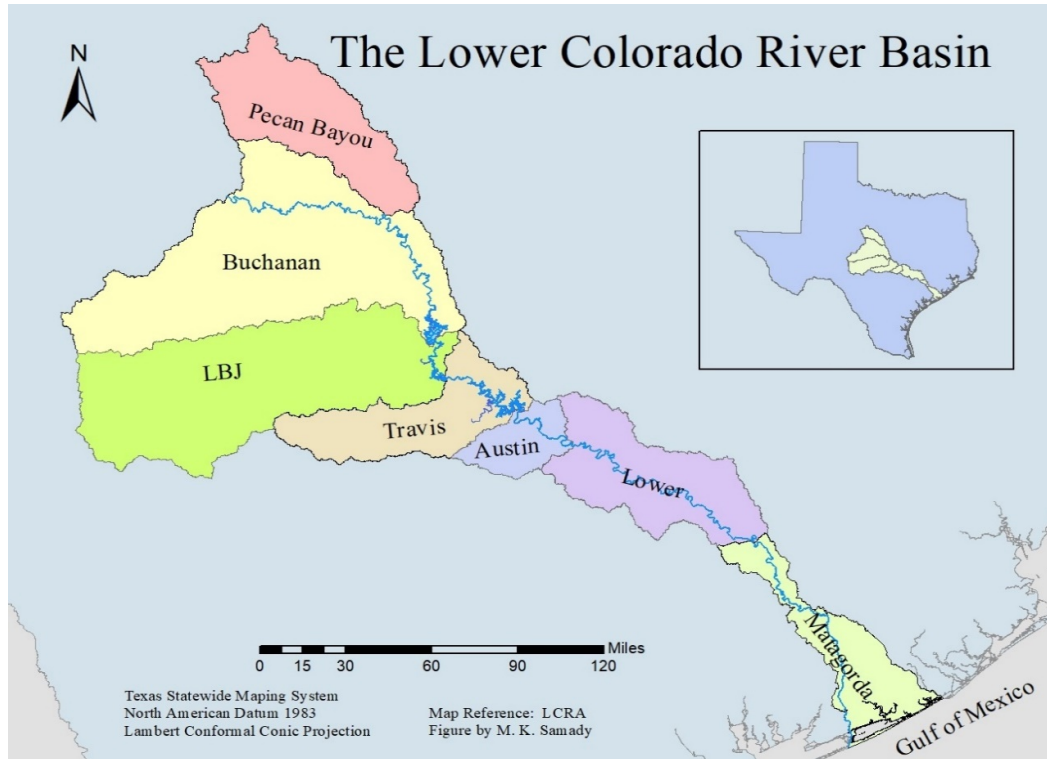
Figure 1: LCRA watershed area map

The LCRA manages and operates six dams on the Colorado River--Buchanan Dam, Inks Dam, Wirtz Dam, Max Starcke, Mansfield Dam and Tom Miller Dam. These dams form six lakes in the upper portion of the watershed, known as the Highland Lakes of Central Texas. The Highland Lakes are Buchanan, Inks, Lyndon B. Johnson (LBJ), Marble Falls, Travis, and Austin. When fully operational, the dams can supply as much as 295 megawatts of electric power (LCRA, 2006). Lake Buchanan and Travis are the two primary water supply reservoirs, and combined they can store as much as 655 billion gallons of water (LCRA, 2017b). The water supplied from these lakes supports over a million people in 55 counties, as well as industries, businesses and the environment. When available, water is also supplied to farmers. Each of the dams on the Colorado River was designed to manage floods, but only Mansfield Dam is operated to hold back floodwaters. Mansfield Dam, which forms Lake Travis, was built between 1937 and 1942

by the U.S. Bureau of Reclamation. Only Lakes LBJ and Travis will be discussed in this study; the other lakes are beyond the scope of this study.

Lake Lyndon B. Johnson (LBJ) is located about 45 miles northwest of Austin. Wirtz Dam was built to form this lake in 1952 to provide additional hydroelectric power per year. This region has a subtropical and subhumid climate, with an average annual precipitation of 24 inches. The Llano River, Colorado River, and Sandy Creek are the major tributaries feeding the lake. Lake Travis was shaped by the construction of Mansfield Dam on the western edge of Austin by the LCRA in 1942, for the primary purpose of floodwater storage. The capacity of Lake Travis is higher than any other Highland Lakes; its surface area is about 1,9297 acres, and it has a volume of 369 billion gallons (LCRA, 2017d). Mansfield Dam is a concrete gravity dam with embankment wings and saddle dikes; it is 278 feet tall, 7089 feet long and 213 feet wide at the base (LCRA, 2017d). It is designed to generate up to 108 megawatts of hydroelectric power.

1.3   Watershed Characteristics

LCRA manages seven sub-basins in the Lower Colorado River Watershed. The basins are Pecan Bayou, Buchanan, LBJ, Travis, Austin, Lower and Matagorda Basins. The flows from first two basins contribute inflows to Lake Buchanan. These flows, along with flows from Lake Travis and LBJ, all contribute to inflows to Lake Travis. Both Travis and LBJ basins are in the Edwards Plateau; these regions are hillier in the south and east; a sharp fault line distinguishes them from adjacent ecological regions. Both basins contain a network of vibrant, cool, continually flowing rivers. Originally covered by Juniper-oak and Mesquite-oak Savannah, a major part of the area is used for grazing beef cattle, goats, sheep, and wildlife (LCRA, 2006). The extents along Lake Travis have experienced some degree of urbanization and land use change recently.

1.4 Climate

The climate in the region is arid in the western part and subhumid in the central part of Texas. The average annual precipitation in the Lake Travis Basin is about 28 inches (711 mm), and it is about 24 inches (610 mm) in the Lake LBJ watershed (LCRA, 2006). Precipitation in central Texas is extremely variable. Precipitation in 2007 was about 65% above the average, while in 2008, the measured precipitation was about 44% lower than the mean annual value. Figure 2 presents a summary of the average monthly rainfall, minimum and maximum monthly temperature, and gross lake evaporation. As can be seen from Figure 2, May, June, and October have higher precipitation compared to the other months, and August, and January have the lowest precipitation amounts. Temperature and evaporation are the highest in June, July, and August.
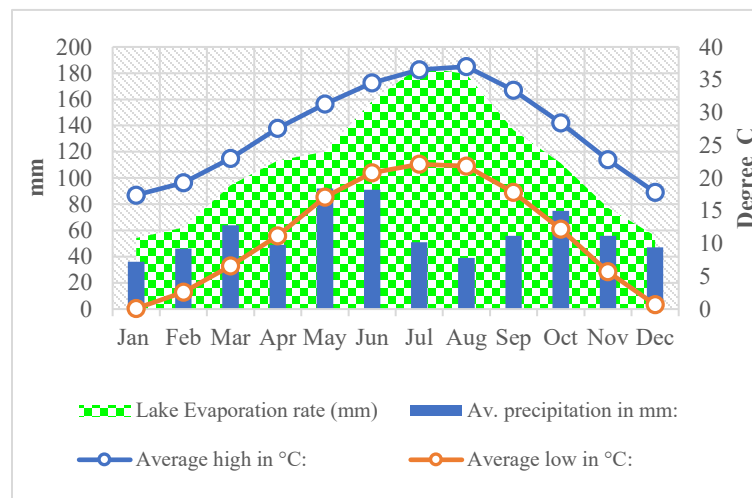
Figure 2- Historical Climate Data Summary
Source: NOAA & US Climate Data

Chapter 2. Review of Hydrological Models

Hydrological models are simplified representations of the actual hydrological cycle that are widely used to help provide sustainable solutions for integrated water resources planning and management. Hydrologic models can be classified based on their capabilities and limitations. According to Chow et al. (1988), hydrological models can be divided into two broad categories, physical and abstract (mathematical). A physically based model is a mathematically idealized representation of real phenomenon, which includes the physical process of the catchment (Devia et al., 2015). Physical models can be further divided into two groups--scale models and analog models. A scale model is a physical representation of the real system that maintains relationships between important aspects of the system; analog models are based on analogous ways to represent the process being studied (i.e., the flow of electricity follows the same fundamental principles as the flow of water).

Models that are developed using logical programming languages and mathematical concepts to explain the land phase of the hydrological cycle in space and time are called abstract (mathematical) models (Jajarmizadeh et al., 2012). According to Shaw et al. (2010) and Chow et al. (1988), a mathematical model can be classified as deterministic or stochastic. In deterministic models, outcomes are determined by known relationships among states and events, without consideration of random variation. In other words, the deterministic model will produce the same output for a single input value and does not account for randomness. In a stochastic model, on the other hand, different values of output can be produced for a single set of inputs that have some randomness. Cunderlik (2003) stated that the deterministic models can be divided into three broad categories-- lumped, distributed, and semi-distributed models. Lumped models treat the catchment as a whole, with state variables that represent averages over the entire basin (Beven, 2001). Distributed models have state variables that represent local averages, in which the

catchment is divided into cells or grid net and flows are passed from one cell (node) to another as water drains through the basin (Xu, 2002).

According to Arnold et al. (1998), distributed models usually require an extensive amount of data for parameterization. Further, Geethalakshmi et al. (2008) stated that due to lack of data, a full understanding of hydrological basins is unachievable via fully-distributed models. However, lumped models do not account for land use and the spatial variability of the hydrological process (Ghaffari, 2011). A model that has some advantages of both types of spatial representation is called a semi-distributed model. The semi-distributed model partly accounts for variation in space with the division of the catchment into sub-basins. This model is more physically based in comparison with the lumped model but requires less data than the fully-distributed model (Jajarmizadeh et al., 2012). This model category can be further divided into event-based and continuous hydrological models. Event-based models account for a single hydrological event, i.e., storm, flood, soil moisture, for a relatively short period of time, while continuous hydrological models simulate multiple state variables (e.g., soil moisture, surface storage) for a longer period.
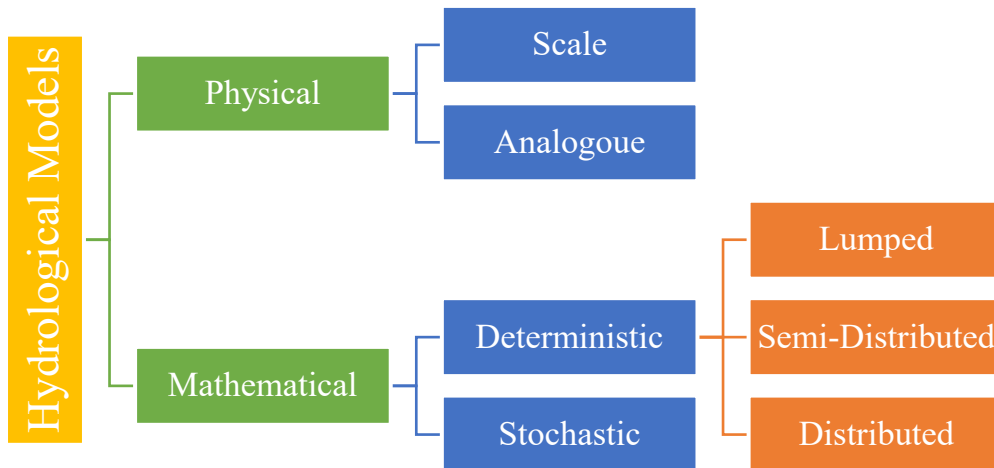
Figure 3: Hydrological Model Classification

2.1 HEC-HMS

The Hydrologic Engineering Center Hydrologic Modeling System (HEC-HMS), developed by US Army Corps of Engineers, is a physically based and deterministic model, primarily applied in a lumped or semi-distributed manner, although it has capabilities for distributed modeling. It is intended to simulate the precipitation-runoff process of dendritic watershed systems (USACE, 2016). HEC-HMS has been used for a variety of purposes, including flood forecasting (Bhuiyan et al., 2017), post-fire response analysis (Cydzik et al., 2009), storm water management (McEnroe, 2010), and climate impact assessment (Meenu et al., 2013). HEC-HMS has the capability to simulate both continuous and event-based hydrological phenomena. The primary distinction is that evapotranspiration and groundwater seepage flow can be ignored for event-based modeling, but not in continuous hydrological modeling. Soil moisture has a significant influence on the hydrological response of a watershed; still, it is rarely tracked in simulation models, due to the complexity of the model structure and challenge of parameter estimation (Holberg, 2015; Tramblay et al., 2010). In HEC-HMS, the Soil Moisture Accounting Algorithm (SMA) and deficit-constant methods are the only loss methods that account for the evapotranspiration process. The SMA loss method simulates the movement of water over time through a set of storage zones in the groundwater and soil profile layers (USACE, 2016). The HEC-HMS with SMA algorithm represents the watershed with five layers and involves twelve parameters. The parameters are surface depression storage, canopy interception storage, soil storage, infiltration rate, tension zone storage, soil percolation rate, storage depth, storage coefficient and percolation rate for shallow and deep ground water layers (Figure 4).
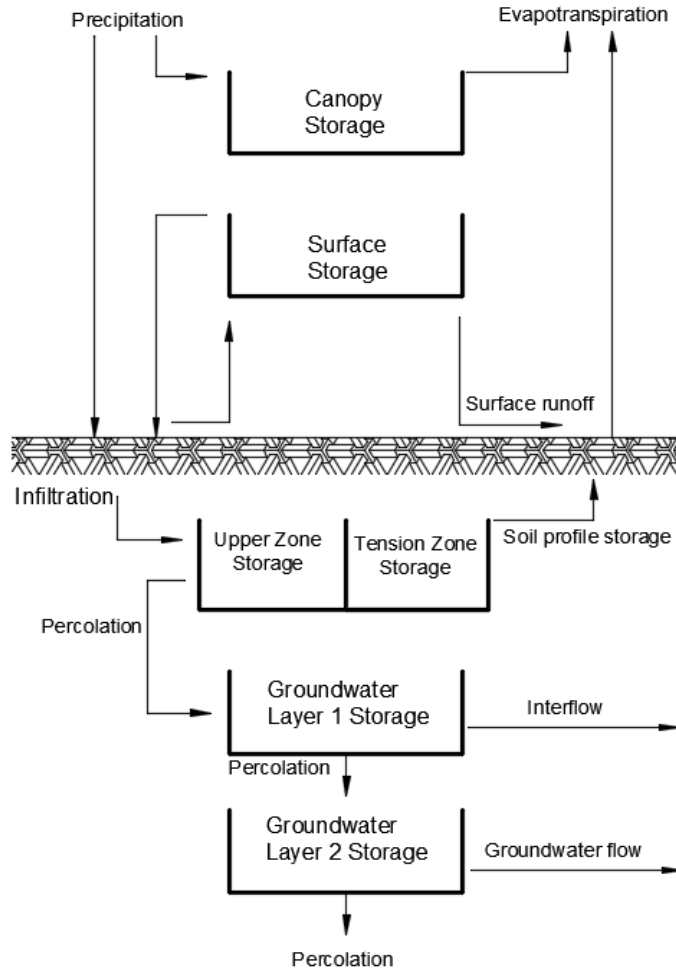
Figure 4: Schematic of soil moisture accounting algorithm in HEC-HMS (Adapted from USACE 2010)

The model takes precipitation as its input and routes it through the canopy, and then it is combined with available surface water storage. If this combination exceeds the potential infiltration capacity of soil profile, the excess volume will become surface runoff. Soil storage is then filled with the infiltrated water volume. Soil storage zone is divided into two parts--upper zone and tension zone storage. Precipitation can percolate from the upper zone, but not from the tension zone, into the first groundwater layer (Holberg, 2015). The water percolated into the topmost ground layer (GW1) will be routed to the

baseflow layer, while the remaining water leaches into the deeper groundwater layer (GW2). The water in GW2 layer then percolates down to a deep aquifer (essentially lost from the system), and the excess water in GW2 routes into the stream as baseflow. The routed water from GW1 and GW2 is transformed to streamflow based on the characteristics of the reservoir, and then it is routed to the basin outlet. The model does not track precipitation and evapotranspiration simultaneously (Bennett et al., 2000). First, it routes precipitation through the system, and evapotranspiration is computed only if water is present in the canopy, surface, or tension soil storage zones and precipitation is not occurring. SMA first calculates the evapotranspiration from canopy storage, then the surface storage. If potential evapotranspiration is not satisfied from the first two storage components, the algorithm removes the water from tension zone storage. Water removal from tension zone occurs at a slower pace based on maximum storage capacity of the tension zone and depth of the soil storage (Holberg, 2015).

2.2 Previous Studies

Several previous studies have addressed drought management in the Lower Colorado River Basin. A multistage stochastic programming model was developed by Watkins et al. (2000) to maximize the revenue of interruptible water and recreational benefits that can support LCRA's decision-making plan. Kracman et al. (2006) further developed this model, aiming to maximize the revenue from rice production and recreation benefits associated with the lake use and hydropower generation. Both of these models used scenario trees based on historical hydrology to represent the uncertainty in reservoir inflows. To incorporate information from climate teleconnections, Wei et al. (2011) developed a probabilistic streamflow forecast model using a polytomous logistic regression method. This statistical model can predict seasonal streamflows into the Highland Lakes reservoir system based on historical sea level pressure and sea surface temperature data. More recently, statistical streamflow forecast models have been

11

developed by the Water Systems & Society Research Group at the University of Wisconsin-Madison (Zimmerman et al., 2016).

At longer time scales, global climate change is projected to have a significant impact on water resources on local, regional and global scales, but it is currently unclear exactly how global climate change will affect precipitation patterns. To understand the long-term effects of climate change on the Lower Colorado River, the LCRA appointed CH2M HILL to develop a physically based watershed model to evaluate future climate change impacts (CH2M, 2008). The Variable Infiltration Capacity (VIC) model was utilized by CH2M HILL to predict long-term inflows into Highland Lakes under a range of scenarios generated by General Circulation Models (GCMs). The model results indicate that under all scenarios the Lake Travis inflows would gradually decline by 2050, and these values would further decrease by 2080 (CH2M, 2008).

Witham (2015) applied the VIC model (Liang et al., 1994) and an associated routing model (Lohmann et al., 1996) to predict season-ahead streamflow in the Lake Buchanan and Lake Travis sub-watersheds. Forecasted meteorological forcings on a 1/8° grid were used to calculate water and energy balances in the watershed. Vegetation cover, soil layers, and elevation bands are inputs that define the physical characteristics of the watershed. The inputs for the routing model include flow directions from each grid cell, the fraction of each grid cell in each sub-basin, the flow routing network, and flow velocity and flow diffusion parameters. Seven soil parameters were adjusted to calibrate the model for the period 1960-1989, and the model was validated over the entire historical period of 1940-2010. The verification results indicated that the model could effectively simulate historical streamflows to Lake Buchanan and Lake Travis. The next step was to run the VIC model with climate ensemble forecasts (hindcasts), to generate seasonal inflow forecasts. By comparing seasonal ensemble mean hindcasts with historical unregulated inflows to Lake Travis and Buchanan, however, it was concluded that the model has little to no skill for season-ahead inflow forecasting, although some skill was found with lead times of 1-2 months. Witham (2015) recommended revising the

12

downscaling method and using more accurate soil moisture data in order to improve seasonal forecasts.

In this study, the widely used HEC-HMS model with soil moisture accounting (SMA) (USACE, 2016) is parameterized, calibrated and verified for the Lake Travis and Lake LBJ sub-basins of the Lower Colorado River. The VIC model is a fully distributed model that requires an extensive amount of data generated in national-level studies and updated periodically ("University of Washington," 2015). In contrast, the HEC-HMS with SMA is a semi-distributed model using data that is readily available from the LCRA, NOAA, and USGS. In addition, as a Linux-based software tool, the VIC model may be less transportable for some users, and it does not have a graphical user interface (GUI), while the HEC-HMS model has a more robust user interface.

Bennett et al. (2000) described the computational steps and formulations used in the SMA algorithm in HEC-HMS. Fleming et al. (2004) derived the soil moisture parameters using the State Soil Geographic (STATSGO) database and geographic information system (GIS) software. Gyawali et al. (2013) used the SMA loss method to examine the performance of HEC-HMS for the snow-affected areas in the Great Lakes region. Holberg (2015) explained the SMA parameterization in detail, and she compared the continuous hydrological modeling technique with event-based modeling methods. This study applies similar soil moisture parameterization methods using the publicly available Soil Survey Geographic Database (SSURGO) to examine the effects of drought on the Lower Colorado River in Texas.

Chapter 3. Methods and Data

This study uses ArcGIS, a Geographic Information System (GIS) software developed by ESRI®, to visualize, analyze, compile, and manipulate spatial information. ArcGIS has several toolboxes that help the users to perform geospatial analysis. For this study, two external toolbars, i.e., Arc Hydro and Geo-HMS were added to ArcMap to facilitate hydrologic modeling process. Arc Hydro is used to delineate and characterize streams and watersheds, calculate drainage properties like slope, flow accumulation, stream network, etc. The Geo-HMS toolbar is used to develop SMA parameters automatically and transfer the data to HEC-HMS from a geospatial environment. Figure 5 shows a schematic of geographic map creation using a combination of layers, with details provided in the following sections.
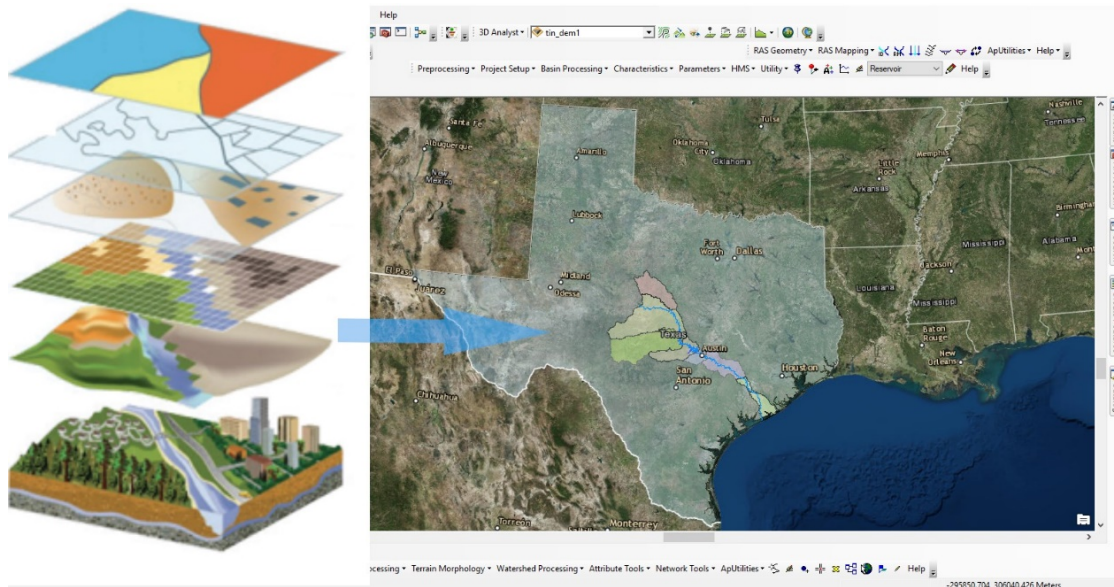
Figure 5: ArcGIS mapping process (figure adapted from ESRI)

3.1   Geospatial Data

A Digital Elevation Model (DEM) is a 3D representation of the terrain surface, represented as a set of equally spaced elevation values (Shellito, 2011). Frequently, DEMs are the primary data used in the analysis of catchment topography for developing hydrological models. For the United States, the USGS National Elevation Dataset is the primary source for DEM data, available at different spatial resolutions. Zhang et al. (1994) and Hutchinson et al. (1991) have explained the effect of grid size on landscape representations. For this study, a 30-m resolution DEM was extracted to delineate the Lake Travis (Pedernales River) and Lake LBJ (Llano River) basins. Watershed boundary shapefiles and stream connectivity data were also used to delineate the watersheds, and this data was downloaded from the Geospatial Data Gateway (GDG) website, https://datagateway.nrcs.usda.gov/.

Land use and land cover data were based on the National Land Cover Dataset (NLCD) 2011, which is provided by Multi-Resolution Land Characteristics (MRLC) consortium. This data was used to determine the Natural Resources Conservation Service (NRCS) runoff curve number, soil properties, impervious surface percentage and canopy storage. Similar to the DEM, the NLCD dataset used for this study has a 30-m grid size (Figure 6).
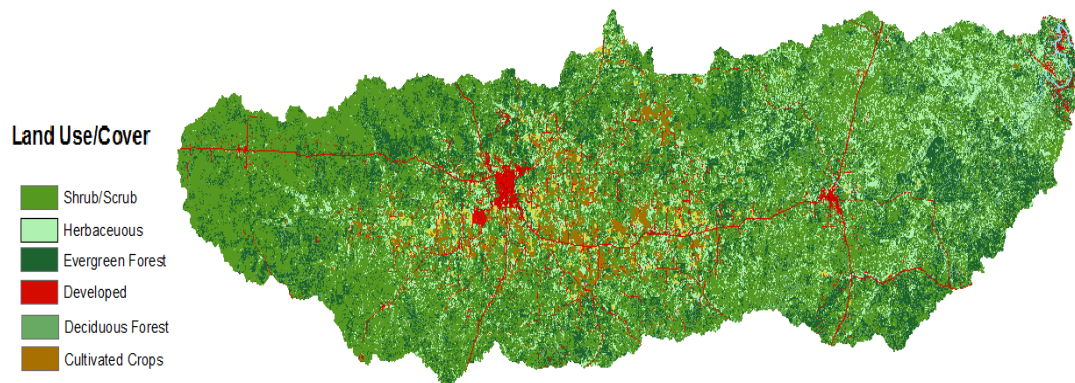
Figure 6: Land use/ land cover map of lower part of Lake Travis Basin

Soils data was based on the Soil Survey Geographic Database (SSURGO) obtained from the United States Department of Agriculture (USDA) webpage, www.websoilsurvey.sc.egov.usda.gov.

3.2 Hydroclimatic Data

Precipitation is the primary hydroclimatic data input to the HEC-HMS model with the SMA algorithm. It was obtained from the National Climatic Data Center (NCDC). Daily total precipitation from the following thirteen gauges were used in this study: 1-Spicewook, 2-Burnet Municipal Airport, 3-Tow, 4-Llano, 5-Gold, 6-Teague Ranch, 7-Fredericksburg, 8-Taylor Ranch, 9-Kerrville 3 NNE, 10-Mason, 11-Harper 3 ENE, 12-Junction Kimble Co Airport, and 13-Junction 4 SSW stations. The average yearly rainfall for 2004-2016 was about 700 mm. The precipitation recorded for 2007 was about 1120 mm, whereas 2011 had the lowest at about 330 mm (see Figure 7).
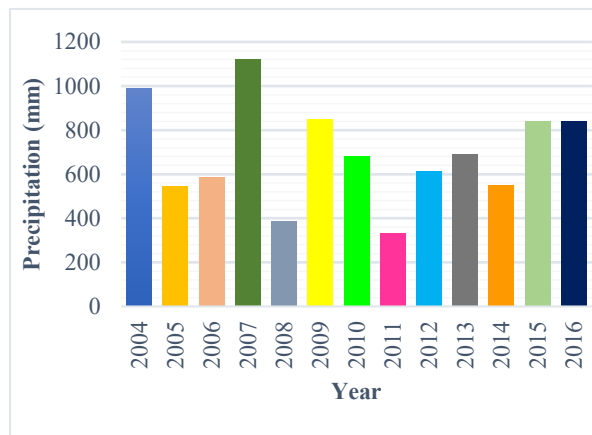
Figure 7: Yearly total precipitation estimated as the average of 13 stations. Source: NOAA

There are eight methods available in HEC-HMS 4.2 for estimating precipitation at the watershed scale (see Table 1). The Gauge Weight (Thiessen Polygon) method is one of the common methods of determining average precipitation for a watershed when there is more than one measurement available. This approach has been suggested by several researchers (Ali et al., 2011; Gyawali et al., 2013; Verma et al., 2010). This approach assigns a weight for each gauge in proportion to its closest basin area. Figure 8 shows the Thiessen polygon network for the study area.

Table 1: Precipitation Calculation Methods in HEC-HMS 4.2

Category	Method
Precipitation	Specified Hyetograph
	Gage Weight (Thiessen Polygon)
	Inverse Distance Gage Weighting
	Gridded Precipitation
	SCS Hypothetical Storm
	HMR 52 Strom
	Frequency Strom
	Standard Project Storm (SPS)
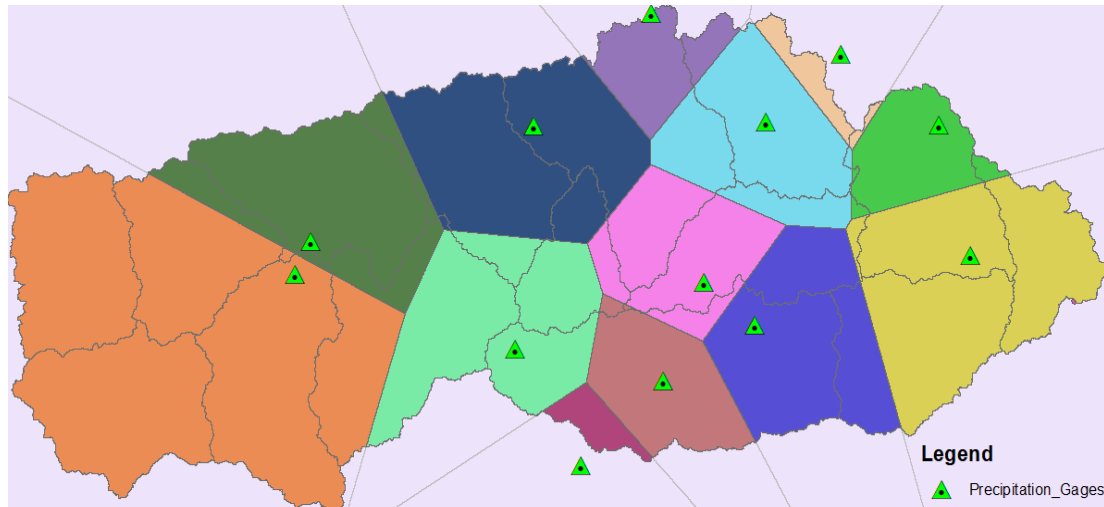
Figure 8: Travis and LBJ basins showing NOAA precipitation gauges and associated Thiessen polygons

The average, minimum and maximum daily temperature data were obtained from the National Climatic Data Center (NCDC) (https://www.ncdc.noaa.gov/). The Austin-Bergstrom International Airport (GHCND: USW00013904) Station was selected for this study, with data obtained for the period 2004-2016. Additionally, relative humidity or dew point temperature are required to estimate evapotranspiration. These data were also obtained from NCDC. Primarily the data was downloaded for an hourly time step, but due to missing data, daily average data was compiled with the precipitation data, the Austin-Bergstrom International Airport (GHCND: USW00013904) Station was selected as for this study, and the data ranged from 2004-2016.

3.2.1   Stream Flow

The two main rivers in the study area are the Llano and Pedernales Rivers. Both of these rivers are tributaries of the Colorado River and drain areas of the Edwards Plateau. The Llano River is about 169 km in length, and the Pedernales River is 171 km long. The

daily flow data from 2004-2016 was obtained from the USGS National Water Information System (http://nwis.waterdata.usgs.gov). The USGS gauges "Llano River at Llano" (08151500) and "Pedernales River at Johnson City" (08153500) were used to calculate the inflow at the catchment outlet

3.3 SMA Algorithm Setup and Parameter Estimation

In addition to building the model schematic in HEC-HMS, the SMA model components must be defined for each sub-basin. As with the meteorological model, HEC-HMS provides several optional methods for each component. Table 2 is a summary of the SMA model components and calculation methods selected for this study.

Table 2: SMA components and calculation methods

Component	Calculation Method
Canopy	Simple Canopy
Surface	Simple Surface
Loss	Soil Moisture Accounting (SMA)
Transform	NRCS Unit Hydrograph
Baseflow	Linear Reservoir
Routing	Muskingum

For these modeling methods, a total of 12 parameters and five initial conditions are required to estimate canopy, soil, surface, and groundwater storage parameters. Seven of the 12 parameters are estimated using soil and land cover databases in GIS. Four

parameters are calculated from streamflow recession analysis, and the final parameter and the initial conditions are calibrated.

Table 3: SMA parameters, data, and estimation methods.

Parameter	Method	Initial Condition	Method
Canopy Storage (mm)	Soil Database	Canopy Storage (%)	Calibration
Surface Storage (mm)	Soil Database	Surface Storage (%)	Calibration
Max Infiltration Rate (mm/hr)	Soil Database	Soil Storage (%)	Calibration
Max Soil Storage (mm)	Soil Database	GW1 Filled Storage (%)	Calibration
Soil Tension Storage (mm)	Soil Database	GW2 Filled Storage (%)	Calibration
Soil Percolation Rate (mm/hr)	Soil Database		
GW1 Storage (mm)	Stream Recession		
GW1 Max Percolation Rate (mm/hr)	Soil Database		
GW1 Storage Coefficient (hr)	Stream Recession		
GW2 Storage (mm)	Stream Recession		
GW2 Max Percolation Rate (mm/hr)	Calibration		
GW2 Storage Coefficient (hr)	Stream Recession		

3.3.1 Evapotranspiration

Evapotranspiration is a combined process of both water vaporization from soil and vegetative surfaces and transpiration through plant canopies. In the SMA model, it is defined as loss of water from the canopy interception, surface depression and soil profile storage (USACE, 2016). HEC-HMS provides seven optional methods for calculating evapotranspiration, including annual and monthly average evapotranspiration, Priestley-Taylor, Penman-Monteith, and evapotranspiration specified for each time step. The Priestley-Taylor and Penman-Monteith methods can also be applied on a grid scale or at the sub-basin level. For this study, the Penman-Monteith method was applied at the sub-basin level. The Penman-Monteith equation approximates net evapotranspiration (ET) based on the combination of energy balance and mass transfer principles. The Penman-Monteith equation is:

$$\lambda ET = \frac{\Delta \left(R_n - G \right) + \rho_a C_p \dfrac{e_s - e_a}{r_a}}{\Delta + \gamma \left(1 + \dfrac{r_s}{r_a} \right)} \qquad (1)$$

where

λ = Latent heat of vaporization

ET = Potential evapotranspiration

R_n = Net radiation (R_{ns} – R_{nl})

R_{ns} = Net incoming shortwave radiation

R_{nl} = Net outgoing longwave radiation

G = Soil heat flux

21

$e_s - e_a$ = Vapor pressure deficit of the air

ρ_a = Mean air density at constant pressure

C_p = Specific heat of the air

Δ = Slope of saturation vapor pressure versus temperature curve (function of temperature)

γ = Psychrometric constant

r_s and r_a = Bulk surface and aerodynamic resistance

Using the Penman-Monteith method, the parameters required to calculate potential ET are wind speed (measured 10 meters above ground level), humidity or dew point, air temperature, and daily solar radiation. The portion of the incident solar radiation not reflected by the surface is the net shortwave radiation (McEnroe, 2010); therefore, shortwave radiation is exclusively associated with the daylight hours for a particular location. The reflected fraction of incident solar radiation is called albedo (α). The albedo is required for computing the energy balance at the surface level. Allen et al. (1998) suggest a default value of 0.23 for reference albedo. The net outgoing longwave radiation is the difference between emitted and reflected longwave radiation.

The FAO56 method is used for the longwave radiation calculation. This approach calculates the infrared radiation based on the Allen et al. (1998) algorithm. The algorithm estimates the solar angle and solar declination for each simulation period, using the geographic location of the watershed, Julian day of the year, and time at the middle of each simulation interval (USACE, 2016).

The Bristow Campbell method was used to estimate the shortwave radiation. Bristow et al. (1984) have stated that during the daylight some portion of the solar radiation would

be blocked by clouds that reduce solar heating as a result reduces the temperature. The inputs for Bristow Campbell method are long-term average temperature, maximum clear sky characteristic over the watershed, which is also called transmittance with the default value of 0.70, and an exponent related to the timing of maximum temperature. The default value for the exponent is 2.4 (USACE, 2016).

Based on the literature review, this study is the first application of a continuous HEC-HMS model with the SMA algorithm using the Penman–Monteith equation combined with the Bristow and Campbell Algorithm and FAO56 solar radiation calculation methods for modeling evapotranspiration. In contrast, other researchers have used monthly average potential evapotranspiration (PET) values. The average monthly PET values are obtained by averaging the historical data, which results in a single value for each month, which may be significantly different than the actual values in locations with high climatic variability. The results of the Penman-Monteith ET calculation used in this study indicate that the PET could vary substantially during different years. For example, Figure 9 shows the calculated PET values for January over the period2012-2016, with .the PET in January 2013 almost double the value in January 2012.
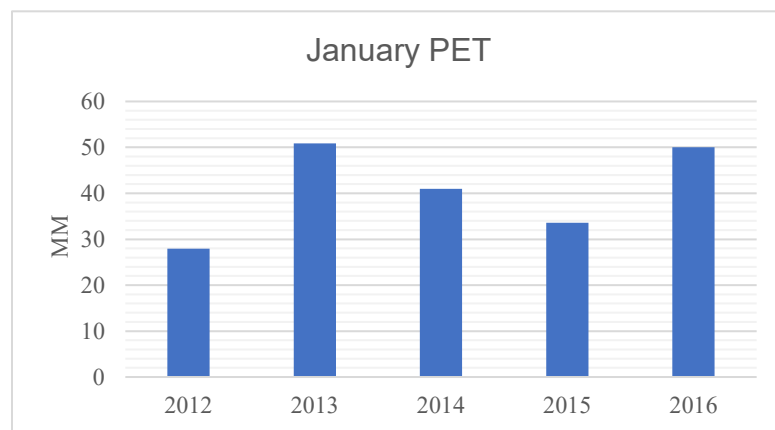
Figure 9: January PET values computed in HEC-HMS with the Penman-Monteith equation.

3.3.2   Parameter Estimation Using NLCD

The precipitation intercepted by vegetation is called canopy interception. The canopy storage capacity varies with the vegetation structure and meteorological factors. Canopy storage can be calculated using NLCD land cover classes (see Figure 23, Appendix A) and canopy interception values provided in Table 4, as suggested by Bennett et al. (2000).

Table 4: Surface slope and depressions. Adapted from Fleming (2002) and Bennett (1998)

Vegetation Type	Canopy Interception (mm)
General Vegetation	1.270
Grasses and Deciduous Trees	2.032
Trees and Coniferous Trees	2.540

The Multi-Resolution Land Characteristics (MRLC) database provides nationwide percent impervious land cover with a 30-meter grid size. All structures such as roads, buildings, bridges, and rooftops are considered as impervious surfaces. Homer et al. (2004) stated that over 76% of the land surface in the United States is classified as having less than 1% impervious cover. The National Land Cover Database 2011 "Percent Impervious" raster file was used for this study to calculate the impervious area for each sub-basin. The results show that only about 0.5% of the area is impervious, because most of the land in the region is covered by farmlands, trees, and shrubs.

3.3.3 Parameter Estimation from NRCS SSURGO

The NRCS Soil Survey Geographic Database (SSURGO) provides detailed soil information on a countywide basis for the United States. The database contains information about surface and soil properties such as water content, erodibility, soil chemistry, soil reactivity, electrical conductivity and much more. Six SMA parameters can be estimated using SSURGO data: maximum surface storage (mm), maximum infiltration rate (mm/hr), maximum soil percolation rate (mm/hr), soil storage (mm), tension zone storage (mm), and percolation rate of the upper groundwater layer (mm/hr). The SSURGO database contains multiple properties tables, and each table contains multiple fields. The fields required to calculate the SMA parameters are summarized in Table 5

Table 5: SSURGO Field Definition Adapted from SSURGO Metadata (2004) and Holberg (2015)

Field Name	Definition	Table	Units of Measure
chkey	Horizon ID		--
cokey	Component ID		--
ksat	Saturated hydraulic conductivity	Horizon	Micrometer/sec
hzdepb	Depth from soil surface to bottom layer		Centimeters
wsatiated	Soil porosity		Percent
wthirdbar	Field capacity		Percent
mukey	Mapunit ID		--
cokey	Component ID	Component	--
comppct	Component percent		Percent
slope	Ground slope		Percent

Soil data are organized on three levels in the SSURGO database: map-units, components, and horizons (Holberg, 2015). A soil map unit is the basic geographic unit that describes the soil types that exist in an area. Each map unit has a unique symbol which is identified and named per the taxonomic classification of the dominant soil or soils (SSURGO, 1995). A map unit can have one or more components. A component is a single soil type, also known as series. Each component has up to six horizons, or soil layers (Figure 10), and each horizon can contain up to 28 soil properties.
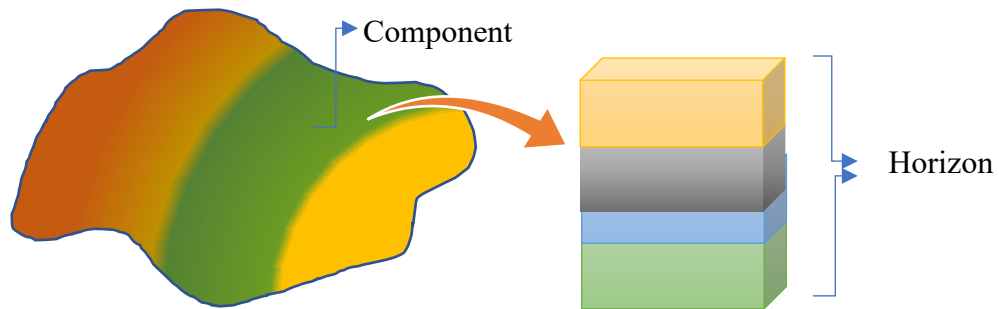
Figure 10: SSURGO database organization (Adapted from Holberg, 2015)

Mukey is a unique map unit identifier which is connected to the information tables in the SSURGO database. The connections between map units, component and the horizon are shown in Figure 11.
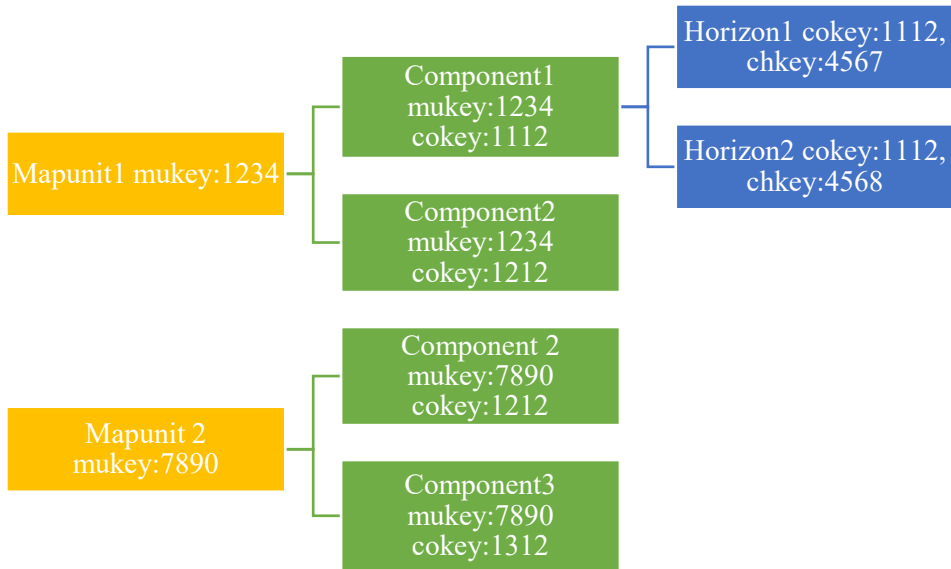
Figure 11: Relationship between map unit, component and the horizon.

3.3.4   Parameter Estimation Using SSURGO

To calculate the SMA soil parameters using the SSURGO database, data preparation in ArcMap and MS Excel spreadsheets is required. Refer to Holberg (2015), "Soil Data Preprocessing" section (p. 26) for detailed data preparation steps.

Surface storage, or surface depression storage, is the volume of water held at the ground surface. The precipitation not captured by the canopy interception can inflow to the surface storage, which can then infiltrate or evaporate. If the inflow exceeds the soil infiltration rate, it will contribute to surface runoff. Bennett et al. (2000) stated that the surface storage capacity is related to the terrain slope and can be estimated from the values shown in Table 6. (See Figure 24, Appendix A for the calculated surface storage raster.)

Table 6: Surface slope and depressions. Adapted from Fleming (2002) and Bennett (1998)

Description	Slope %	Surface Storage (mm)
Paved Impervious Area	NA	3.18-6.35
Flat, Furrowed Land	0-5	50.8
Moderate to Gentle Slopes	5-30	6.35-12.70
Steep, Smooth Slopes	>30	1.02

As demonstrated in the SMA algorithm schematic, the soil profile is divided into two parts--the upper zone and the tension zone. The upper zone loses water due to ET and percolation, while the tension zone loses water only due to ET. The ET losses in the upper zone are assumed to occur prior to the tension zone. Another assumption is that the water is removed from the system at a one-to-one ratio if the current soil storage exceeds 60% of the maximum tension zone storage, as shown in Figure 12.
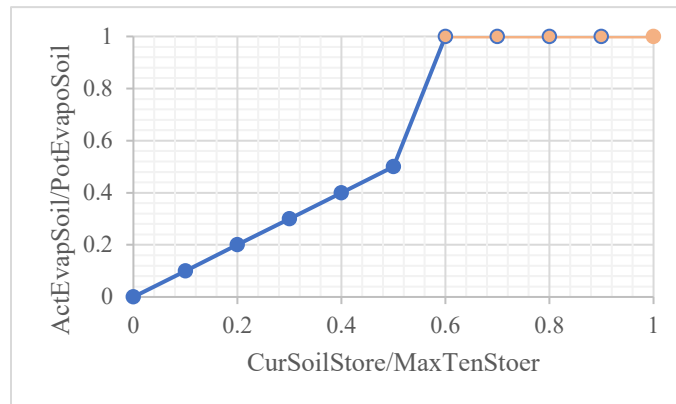
Figure 12: Actual ET for the Tension Zone. Adapted from Bennett (2000)

An example calculation of maximum soil storage is as follows, accounting for both upper zone and tension zone storage.

Mapunit: 58125

Cokey 11441916   Cokey 11441917

Component (%) 20   Component (%) 75

Porosity (%) 27.6   Porosity (%) 16.7

Depth from Soil Surface (cm) 97   Depth from Soil Surface (cm) 56

$$\text{Maximum Soil Storage} = \left(\frac{20}{100} * \frac{27.6}{100} * 97\right) + \left(\frac{75}{100} * \frac{16.7}{100} * 56\right) = 12.3 cm$$

The calculated soil storage raster is shown in Appendix A (Figure 26).

The highest rate at which precipitation can enter the ground from the ground surface is the maximum infiltration rate. The amount of infiltration is a function of the volume of water available for infiltration and maximum infiltration rate calculated from SSURGO. The hydraulic conductivity increases as water content increases to saturation, so the hydraulic conductivity is maximum when the soil is saturated (Dingman, 1994). However, the saturated hydraulic conductivity is the lower bound of the maximum infiltration rate, because infiltration is also driven by capillary tension in the soil. In this study, the maximum infiltration capacity was estimated using the weighted average of the first soil layer's hydraulic conductivity, which was obtained from SSURGO database, as a lower bound. An example calculation of this lower bound is shown below.

<div align="center">

Mapunit: 58125

</div>

Cokey 11441916	Cokey 11441917
Component (%): 20	Component (%): 75
Layer1 saturated hydraulic conductivity (μm/s): 2.7	Layer1 saturated hydraulic conductivity (μm/s): 0.3

Maximum Infiltration Rate $= \left(\frac{20}{100} * 2.7\right) + \left(\frac{75}{100} * 0.3\right) = 0.765 \ \mu m/s$

The calculated soil storage infiltration is shown in Appendix A (Figure 25).

The maximum percolation rate is the highest rate at which water enters the soil profile, ground layers, and deep aquifer. Following Bennett et al. (2000) and Fleming et al. (2004), the maximum percolation rate is calculated from the average saturated hydraulic conductivity for all the layers of the soil component.

<div align="center">

Mapunit: 58125

</div>

Cokey 11441916	Cokey 11441917
Component (%): 20	Component (%): 75
Average saturated hydraulic conductivity (μm/s): 5.2	Average saturated hydraulic conductivity (μm/s): 30.4

$$= \left(\frac{20}{100} * 5.2\right) + \left(\frac{75}{100} * 30.4\right) = 23.84 \ \mu m/s$$

The water stored in capillary zone storage or pores of the soil represents the tension zone storage. The maximum tension zone storage is calculated using field capacity multiplied by the depth of each soil layer for each component.   A sample calculation is as follows:

	Mapunit: 58125	
Cokey 11441916	Cokey 11441917
Component (%) 20	Component (%) 75
Field capacity (%) 13.6	Field capacity (%) 7.3
Depth from Soil Surface (cm) 97	Depth from Soil Surface (cm) 56

$$= \left(\frac{20}{100} * \frac{13.6}{100} * 97\right) + \left(\frac{75}{100} * \frac{7.3}{100} * 56\right) = 5.7 \ cm$$

3.3.5   Parameter Estimation Using Streamflow Recession Analysis

Groundwater layer 1 and 2 storage coefficients and storage depths were estimated using the recession analysis method suggested by Fleming (2002). Hydrographs for five independent storms events for the Llano River at Llano were analyzed for this process. A typical hydrograph can be divided into three parts: rising limb, peak, and falling limb, or recession. The recession curve or the depletion curve represents the water withdrawal from the basin storage. Linsley et al. (1958) stated that the surface inflow to the channel system stops at the inflection point on the receding limb of the hydrograph. The following function suggested by Fleming et al. (2004) was used to estimate the recession coefficient and groundwater storage.

$$q_t = q_o * K_r = q_o * e^{-at} \qquad\qquad (2)$$

where q_0 is initial streamflow, q_t is the stream flow at the time t, K_r is a recession constant for the period between time 0 and time t, and $a = -lnK_r$. Linsley et al. (1958) propose a one-day time interval for streamflow recession analysis. The basin storage formulation can be obtained by integrating equation (2) and noting that during the time interval dt the volume of the discharged water is equal to $q * dt$, which is equivalent to reduction in storage $-dS$ for the same time interval.

$$S_t = -\left(\frac{q_t}{\ln K_r} \right) = \frac{q_t}{a} \qquad (3)$$

where S_t is the basin storage at the time t. By dividing the storage volume over the basin area, the basin storage capacity can be obtained. Refer to Linsley Jr et al. (1975) for a detailed description of streamflow parameter analysis.
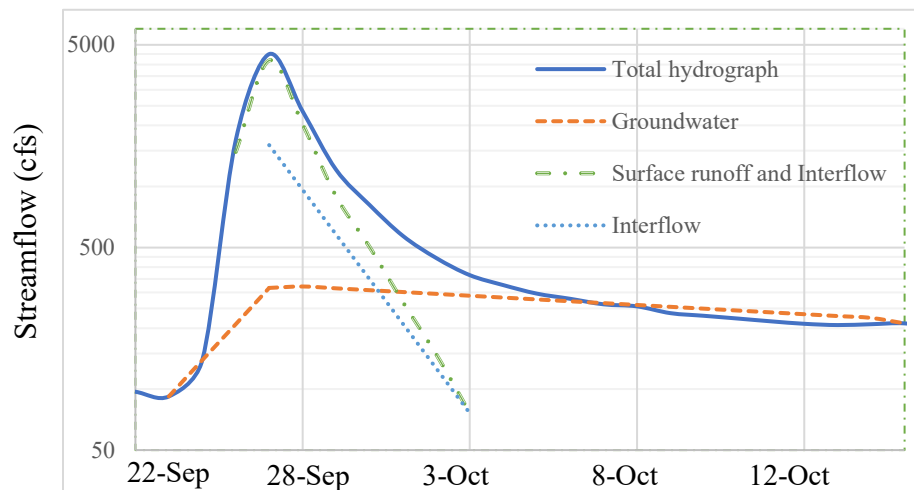
Figure 13: Stream Recession Analysis

Five isolated storm events for three different years were analyzed at this stage (see Figure 13 for an example). Based on these five estimates, average groundwater recession

coefficients and maximum storage values were obtained for the baseflow and interflow. Table 7 summarizes the calculation results for the Llano River baseflow and interflow parameter estimation. (See Appendix C, Table 11 for the results for each storm.)

Table 7: Streamflow Recession Analysis

Parameter	Value
Baseflow Storage (mm)	7.5
Baseflow Coefficient (hr)	1038
Interflow Storage (mm)	1.7
Interflow coefficient (hr)	52

Chapter 4. Results

4.1 Preliminary Simulation Results

The primary purpose of model parameterization and calibration is to simulate the observed flows into the Highland Lakes. The flow into the lake is represented by flow at the catchment outlet, but this point does not have a specific flow gage. One reason that there is no flow gauge right at the inlet to the lake is that water levels in the lake fluctuate, and the backwater effects would impact flow measurements. Thus, the LCRA uses the following area-weighted formula to estimate the monthly flows into the lake, based on gauge measurements some distance upstream.

$$Q(t) = 1.19 * Q(l) + 2.14Q(p) \qquad (4)$$

where $Q(t)$ is the total inflows to the Lake Travis, $Q(l)$ is the streamflow observed at the Llano River gage (USGS 08151500), and $Q(p)$ is the flow observed at the Pedernales River near Johnson City gage (USGS 08153500).

McEnroe (2010) stated that the ideal simulation time period for evaluating hydrological models is a decade or more, to average out the year-to-year variability. However, a short computation time step is recommended to capture the watershed response to rainfall events, and the NRCS guidelines suggest that the computational time step should not exceed 29% of the watershed lag time USACE (2000). Accordingly, the test period for this study extends from January 1, 2004, through December 31, 2016, and a 1-hour time step is used for model computation. The test simulation period was used to check the initial performance of the model, based on the estimated parameters from the GIS-based and time series calculations. The preliminary simulation results showed that the model tended to overestimate the peak flows and runoff volume.

To decrease the simulated runoff volume and improve the peak sharpness, a manual calibration approach was deemed necessary. The model was calibrated for the period of 2004-2012 and validated for the period of 2012-2017. Only two model parameters were adjusted in the calibration. The percent streamflow volume error, PVE, is used as the primary metric for the objective function (Jain et al., 2003). In addition, a set of hydrological model performance efficiency criteria such as the coefficient of determination (R^2), percent bias (PBIAS), and the Nash-Sutcliffe Efficiency coefficient NSE (Nash et al., 1970) was used to evaluate the model performance.

The percent deviation of streamflow volume (PVE) indicates the overall agreement between the observed flow and simulated flow over a specified time interval.

$$PVE\% = \frac{Q_{obs} - Q_{sim}}{Q_{obs}} * 100 \qquad (5)$$

where Q_{obs} is the observed streamflow (m^3/s) and Q_{sim} is the simulated streamflow (m^3/s) at the watershed outlet.

Percent bias (PBIAS) compares the average tendency of the simulated flows to be larger or smaller than the observed flow values (Gupta et al., 1999)

$$PBIAS(\%) = \left[\frac{\sum_{i}^{n}(Q_{obsi} - Q_{simi}) * 100}{\sum_{i=1}^{n} Q_{obsi}} \right] \qquad (6)$$

Nash-Sutcliffe Efficiency (NSE) is calculated using Equation (7)

$$NSE = \frac{1 - \left[\sum (Q_{obs} - Q_{sim})^2 \right]}{\left[\sum (Q_{obs} - \overline{Q}_{obs}) \right]} \qquad (7)$$

where $\bar{Q}_{obs}$ is average observed streamflow.

Pearson's coefficient of determination indicates the collinearity between simulated and observed data (Moriasi et al., 2007).

Recommended performance ratings of watershed models based on the above statistical parameters are summarized in Table 8, adapted from Moriasi et al. (2007) and Jain et al. (2003). The PBIAS and NSE ranges were suggested by Moriasi et al. (2007) based on his literature review.

Table 8-: General performance ratings for watershed models

Performance Rating	R^2	PBIAS / PVE	NSE
Very Good	$0.75 < R^2 \leq 1$	$PBIAS < \pm 10$	$0.75 < NSE \leq 1$
Good	$0.65 < R^2 \leq 0.75$	$\pm 10 \leq PBIAS < \pm 15$	$0.65 < NSE \leq 0.75$
Satisfactory	$0.75 < R^2 \leq 0.65$	$\pm 15 \leq PBIAS < \pm 25$	$0.50 < NSE \leq 0.65$
Unsatisfactory	$R^2 \leq 0.5$	$PBIAS \geq \pm 25$	$NSE \leq 0.5$

4.2 Calibration Results

The results of a sensitivity analysis showed that the maximum soil storage, maximum infiltration rate, tension zone storage, baseflow (GW2) storage, and deep percolation rate had more effect on simulation results compared to the other parameters. To minimize the calibration parameters and not overfit, only the interflow storage capacity (GW1) and the deep percolation rate (GW2) parameters were adjusted during the model calibration. The GW2 percolation rate is a conceptual parameter with high

sensitivity, and thus it is often selected as a calibration parameter. In the previous chapter, it was stated that the interflow storage depth shows variability during the different storm events. Fleming (2002) and Holberg (2015) indicated that the interflow and the baseflow variables do not behave uniformly throughout the year. To represent the seasonal variability of the watershed, they suggested dividing the model into seasonal or semi-annual simulation intervals. However, in another study, Gyawali et al. (2013) used a single parameter estimation approach for the different variables throughout the calibration and validation time frame. In this study, the same parameter estimation approach as suggested by Gyawali et al. (2013) is followed, but with fewer calibration parameters and a longer simulation time span.

The calibrated model parameters for all fifteen sub-basins are summarized in Table 9. The estimated and calibrated parameters obtained in this study were compared with those from similar studies (Gyawali et al. (2013) Fleming et al. (2004); Holberg (2015); and McEnroe (2010)), and it was found the estimated parameters are generally in the same range, except the impervious surface values are lower than the values used in other studies. This is because over 99% of the land cover of the region in this study is covered with vegetation and trees; and less than 1% of the land surface is covered by asphalt, concrete and other impervious materials.

Table 9: Range of the parameters after calibration

Parameter	Minimum	Maximum	Average
Max. Canopy storage (mm)	2.02	2.31	2.22
Max. Surface storage (mm)	5	45	34
Max infiltration (mm/hr)	19	70	38.3
Surface Impervious %	0.07	2.94	0.47
Soil storage (mm)	66	240	131
Tension storage (mm)	43	171	89.2
Soil percolation (mm/hr)	15	66	35
GW 1 Storage (mm)	3	3	3
GW 1 Percolation Rate (mm/hr)	8	32	17.8
GW 1 Storage Coefficient (hr)	52	52	52
GW 2 Storage (mm)	40	40	40
GW 2 Percolation Rate (mm/hr)	0.25	0.28	0.278
GW 2 Storage Coefficient (hr)	1040	1040	1040
Lag Time (minutes)	427	908	603

To demonstrate the model performance using the calculated and calibrated SMA parameters, the results for one of the basins are shown in Figure 14. It can be seen that the soil infiltration follows the same pattern as precipitation, as expected. The amount of soil infiltration is related to the availability of water and the infiltration capacity of the soil. The infiltration capacity is maximum at the initial stage; it decreases exponentially

before it reaches the equilibrium condition. The total infiltration should always be less than or equal to the precipitation amount if precipitation is the only source of water, which is the case in Texas where snow accumulation and melt are negligible. It can be seen from Figure 14 that the total monthly precipitation is lower or equal to the infiltration in each month except for July 2007. This may be due to the June 2007 precipitation rate exceeding the infiltration rate, with some of the excess water filling surface storage and allowing infiltration to continue after the storm events ended.
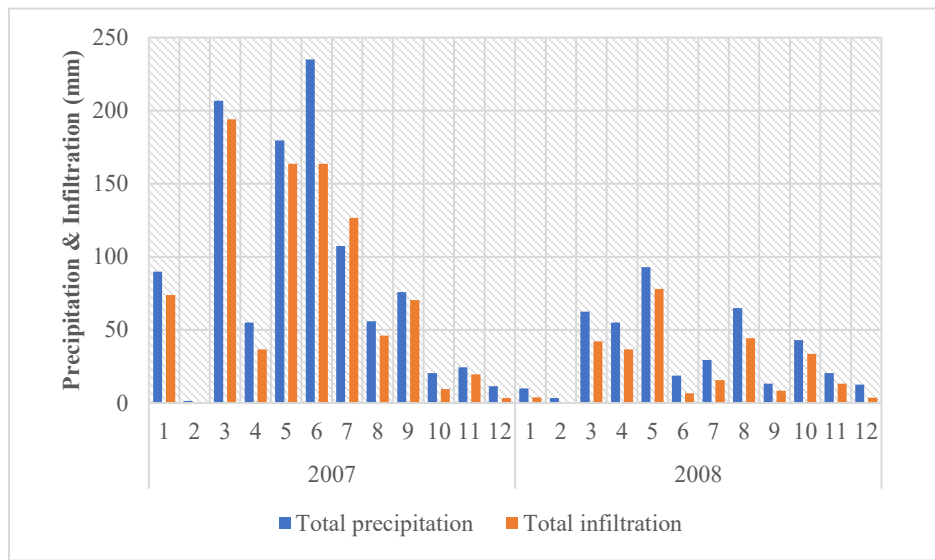
Figure 14: Total monthly precipitation and infiltration (mm) for a wet year (2007) and dry year (2008)

The monthly average canopy interception is shown in Figure 15. The amount of precipitation stored in the canopy is affected by the storm hydrograph, vegetation type, and time of the year (Ponce Victor, 1989). Figure 15 demonstrates the monthly average canopy interception follows the precipitation pattern during 2007 and 2008, as expected.
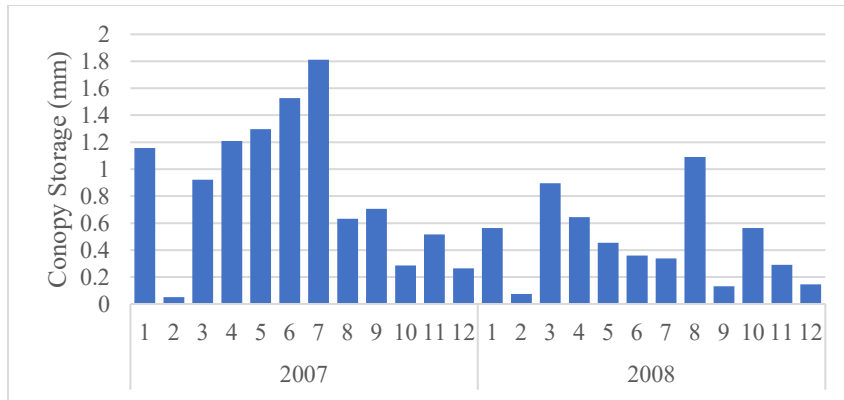
Figure 15: Average monthly canopy storage (mm)

The upper zone soil storage and the tension zone soil storages were defined based on the soil porosity, soil depth, and depth to the water table. Figure 16 shows the fluctuation of total soil storage and saturation fraction. Overall, this demonstrates the high soil storage that can occur during wet periods, and the low soil storage resulting from dry periods, as well as the rate at which the soil can dry.

Figure 16: Total monthly soil storage and soil saturation fraction

4.3 Sensitivity Analysis

The impact of each parameter was determined through a sensitivity analysis. Three sub-basins were selected to analyze the variability of flow at the outlet. The value of each parameter was increased by 10%, holding the other parameter values co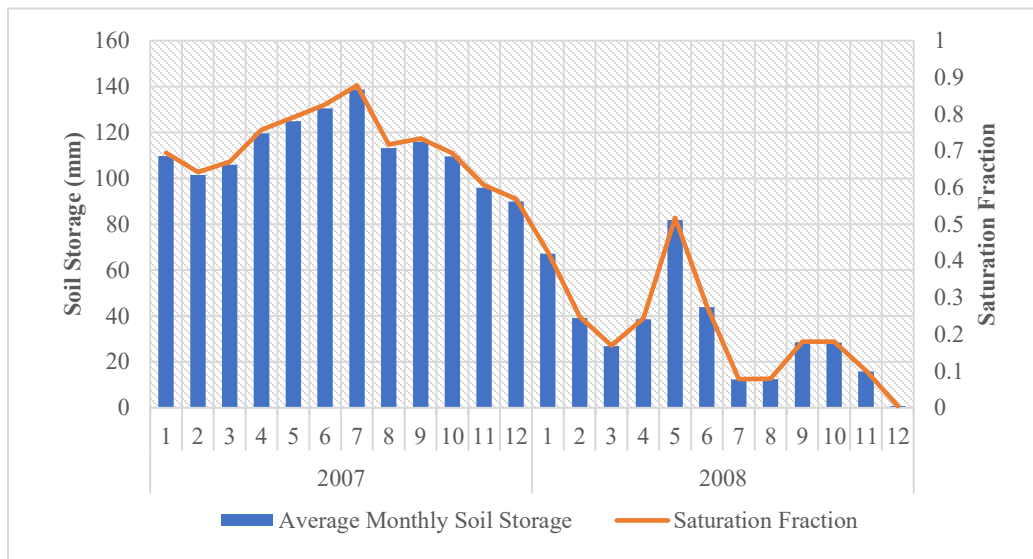nstant, and the percent change in the total discharge values at the outlet of each sub-basins was recorded. The average percent change values are shown in Figure 17. The positive values indicate that a 10% increase in the parameter led to an increase in the discharge at the outlet of the sub-basin, while the negative values indicate a reduction in the discharge at the outlet of the sub-basin. Based on this analysis, varying the GW2 percolation rate had the highest impact, while varying the maximum infiltration rate had the lowest impact on the total streamflow discharge. However, each parameter has a different effect on the components of total discharge (runoff, interflow, and baseflow), which may be further explored in future research.
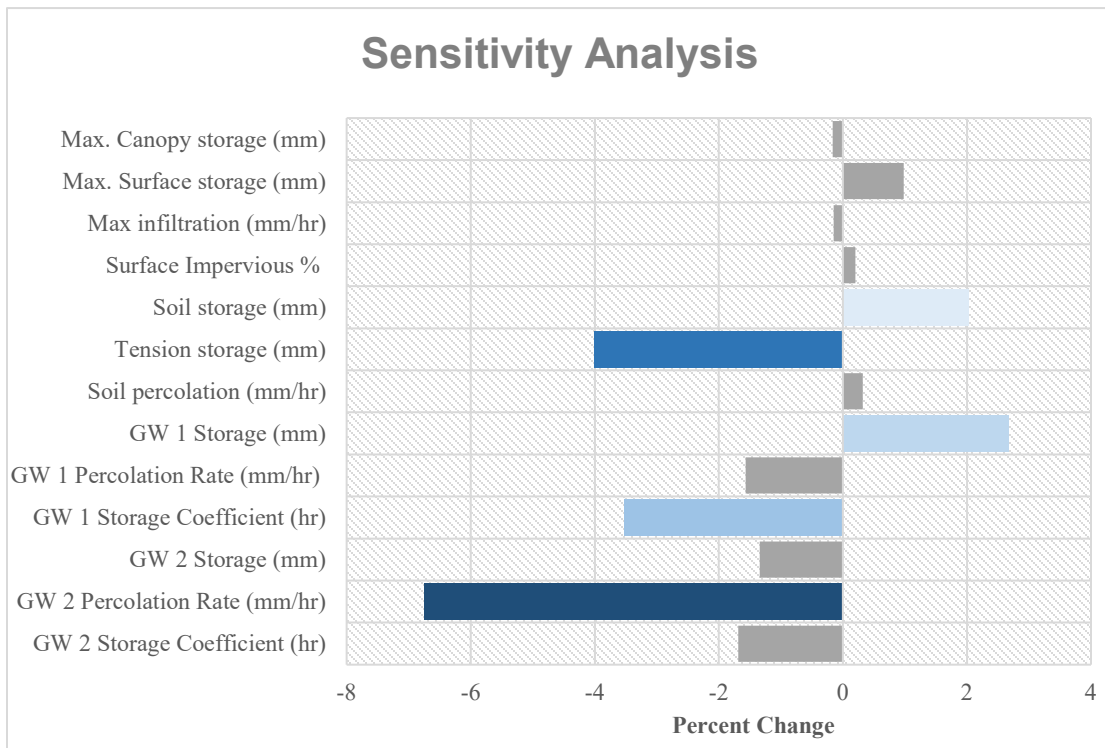

Figure 17: Results of the sensitivity analysis

4.4 Final Simulation Results

Figure 18 shows a time series comparison between the simulated flows and observed flows at the watershed outlet point during the calibration period. The hydrograph comparisons indicate that the HEC-HMS captures the baseflow relatively well at a monthly time step, but at daily or hourly scales, it can be seen that the model underestimates the baseflow for the low flow period periods. The HEC-HMS model also captured the time-of-peak reasonably well, with the difference between the observed and simulated values typically being a day or less (see Appendix D). This difference might be due to the routing coefficients (K) or using daily streamflow and simulating at an hourly time step.
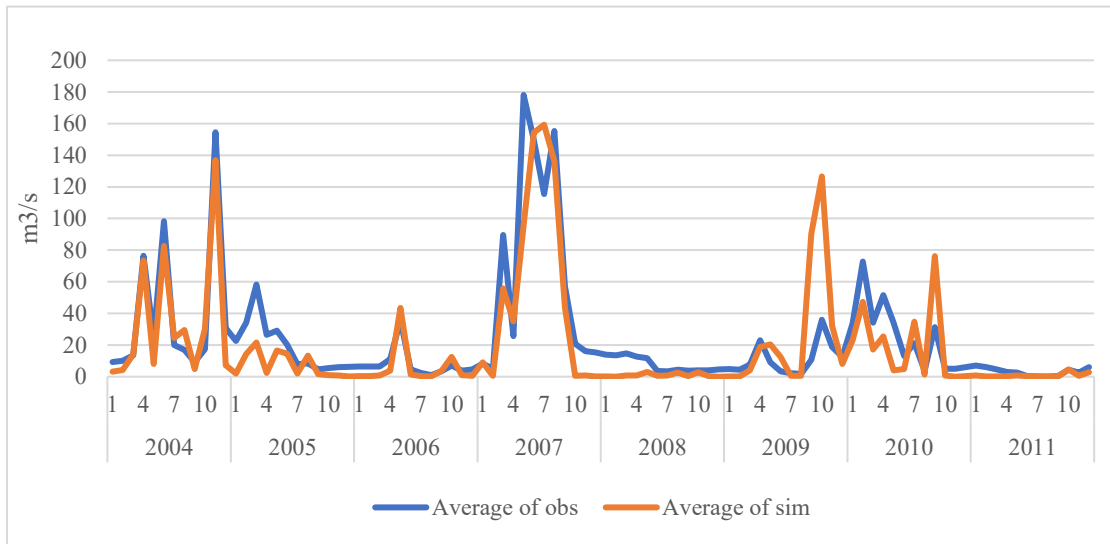
Figure 18: Observed and simulated monthly hydrographs for the calibration period (2004-2012)

Time series comparisons between the simulated and observed streamflows during the validation (testing) period are shown in Figures 19 and 20. The hydrograph comparison indicates that the HEC-HMS model performed well in matching the observed streamflows during the validation period, although there is some shift in the peak flows. During the high flows in May and June 2015, both hydrographs matched closely at the

start, but the simulated streamflow hydrograph overestimates the peak flow and recession, and lags the observed streamflow hydrograph. Overall, both hydrographs follow the same pattern during the low and high flow periods. (See Appendix D, Table 13 for data.)

Figure 19: Observed and simulated hydrographs for the validation period

Figure 20: Daily average observed and simulated hydrographs for the validation period

The statistical measures of HEC-HMS model performance are summarized in Table 10. The percent volume error (PVE) calculates the volume difference bet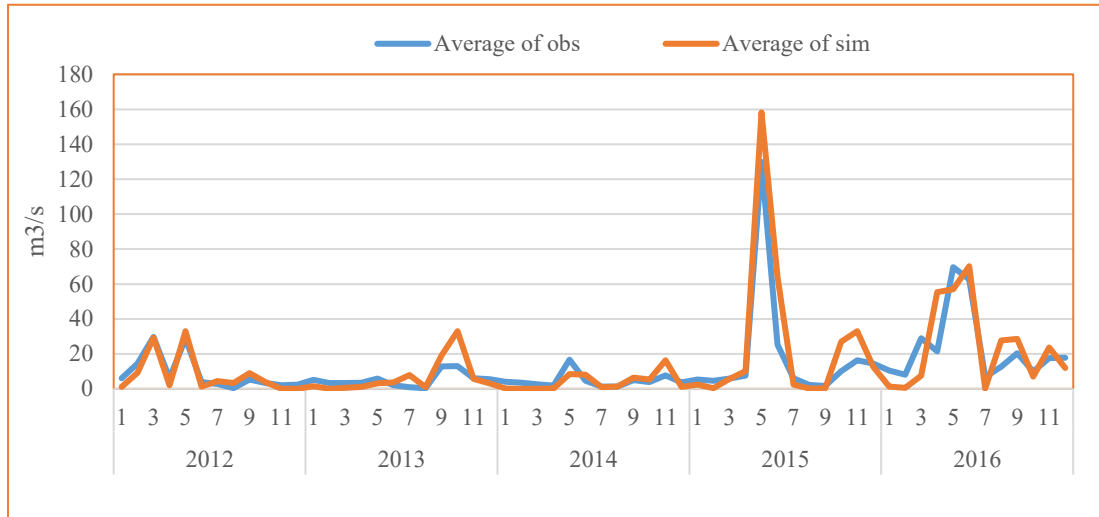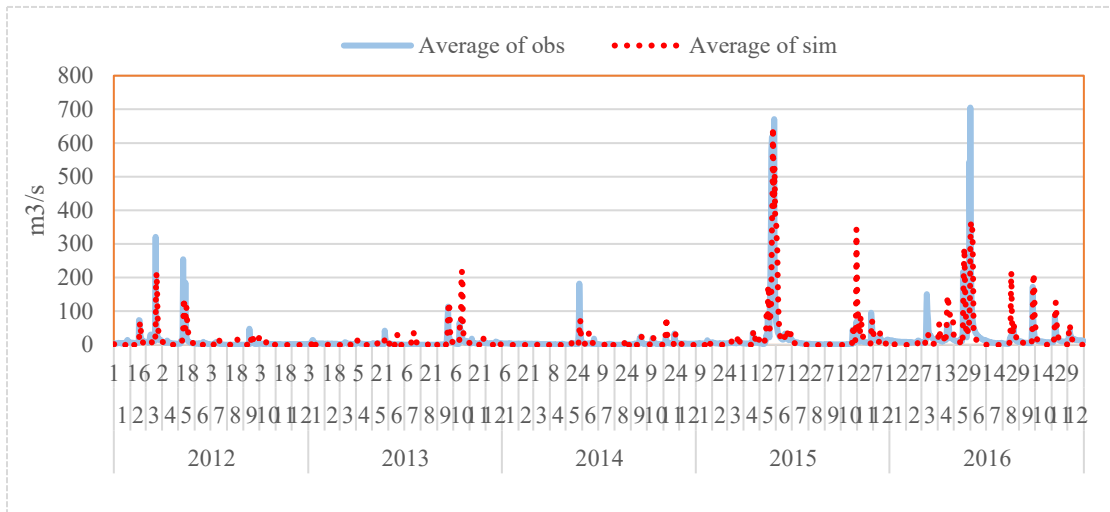ween simulated and observed streamflows, with a positive value indicating that the model underpredicts observed flows (see Eq. 5). This model underestimated the observed flow by less than 17% during the calibration period and overestimated flow by 12.6% during the testing period, but over the entire period, it underestimated the observed streamflows by about 9.6%. Overall, based on the PBIAS, model performance rates from good to very good.

The Nash-Sutcliff efficiency factor calculates the difference between the observed and estimated values as a squared value. The Nash-Sutcliff coefficient varies from 0.7 to 0.73, which indicates the model performance is good.

Finally, according to the coefficient of determination (R^2), there is a relatively good correlation between the simulated flows and the observed streamflows at the catchment outlet.

Table 10: Performance assessment of the HEC-HMS model

Metric	Calibration Period (2004-2012)	Validation Period (2012-2017)	Entire Period (2004-2017)	Performance Rating
PBIAS (%)	17.0	-12.6	9.6	Very Good
NSE	0.70	0.73	0.71	Good
R^2	0.73	0.86	0.74	Good

In addition to the standard metrics in Table 10, the cumulative distribution function (CDF) and the cumulative flow deficit (CFD) time series were plotted to evaluate the model's performance with focus on low flows, or drought periods. The CFD curves for the observed and simulated flows are shown in the Figure 21. It can be seen that about

60% of the flows are below 10 m^3/s for the both observed and simulated flows. However, 40% of the simulated flows are below 1 m^3/s, while flows below 5 m^3/s are observed at this frequency, indicating that model performance can be further improved for low-flow periods.
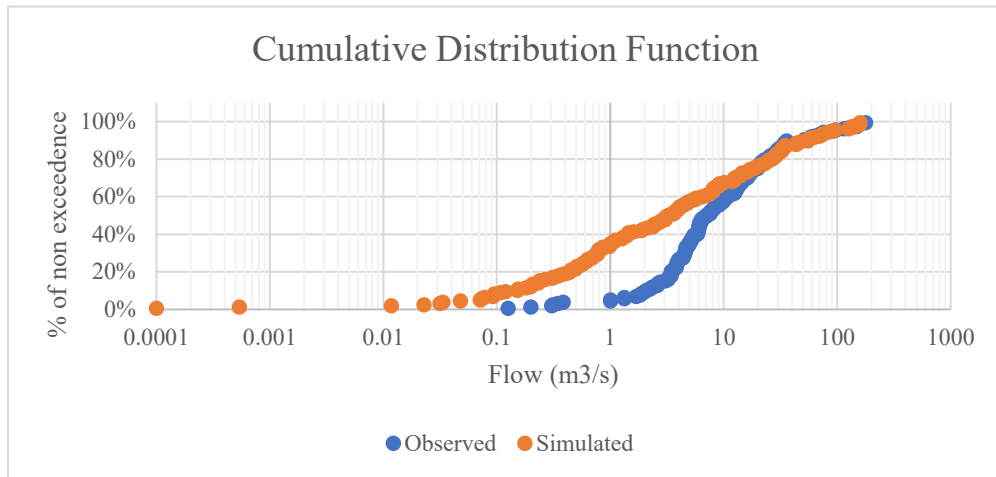
Figure 21: Cumulative distribution function of streamflow at the outlet
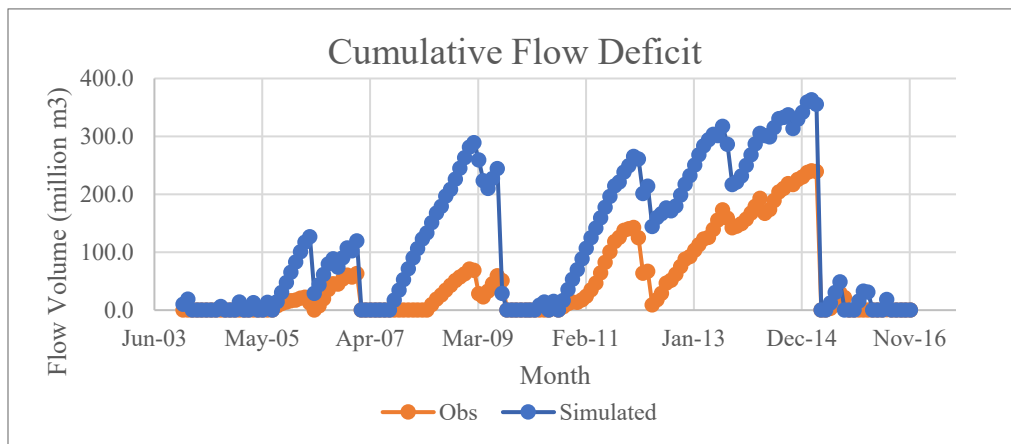
Figure 22: Cumulative flow deficit graph

To compute the cumulative flow deficit time series, a reference flow volume is required to compute the flow deficit (Zelenhasić et al. (1987). Due to the high water demands in

the Lower Colorado River Authority, the median (50th percentile) of the measured streamflow is used as the reference value. The CFD time series for the observed and simulated flows for the entire period are plotted in the Figure 22. As can be seen, the flow deficit of the simulated model is consistently higher than the measured streamflow, which is the result of the model under-estimating the low flows. These low flow values are difficult to compare from the hydrograph comparison, but analysis of the CDF and CFD show that the model tends to exaggerate the effects of drought on streamflow. Further calibration is required to improve model performance for the low flows.

Chapter 5. Conclusions

The objective of this study was to develop and parameterize a continuous HEC-HMS model with soil moisture accounting for the Highland Lakes in Central Texas. This study shows that the soil moisture parameters for the SMA algorithm can be derived from the Soil Survey Geographic Database (SSURGO) and streamflow records. The ArcGIS software and HEC-GeoHMS toolkit were used to facilitate the parametrization process. Historical daily precipitation, temperature, wind speed, and humidity data were used to calculate the water-balance and energy flux over the entire watershed. Based on the literature review, this study is the first application of a continuous HEC-HMS model with the SMA algorithm using the Penman–Monteith equation combined with the Bristow and Campbell Algorithm and FAO56 solar radiation calculation methods for modeling evapotranspiration. In addition, this model accounts for spatial hydrologic variability in more sub-basins and the analysis of results also focuses on drought impacts.

This study revealed that the soil moisture parameters could have a significant impact on the streamflow runoff and peak flows, with the deep (GW2) percolation rate being the most sensitive calibration parameter according to a sensitivity analysis.

Despite parameter uncertainty, the HEC-HMS model was shown to simulate the historical streamflow at the Lake Travis catchment outlet reasonably well. The model simulated the extreme events very well; it demonstrated both wet years and dry years. The rising limb of the simulated and observed peak flow hydrographs match reasonably well, but the recession limb of modeled flows tended to be higher than the observed flows. The results of statistical analysis showed that the simulated values were well correlated with the measured flow and the percent volume difference was about the minimum. The Nash-Sutcliff efficiency parameter is 0.7 for the calibration period, 0.74 for the validation period and 0.71 for the entire simulation period

This study has a number of limitations. One significant limitation related to the hydrological model is the spatial and temporal variability of the climate data (precipitation, temperature, wind speed, and humidity). The HEC-HMS model assumes a uniform climate throughout the sub-catchments, while in reality, climate variables vary between the gauges. This is particularly important for precipitation, as the hydrological model might overemphasize a small storm event occurring upstream of the rain gage, while local rainfall events occurring between the gauges might not be recorded by the gage station.

The majority of the storm events in central Texas end in a few hours, with very few continuing for a day. However, daily precipitation and streamflow data were used for this study. The HEC-HMS simulation time interval was set to hourly because the NRCS suggests that the time step should not exceed 29% of basin lag time, which led to a time interval mismatch that may affect the simulated hydrograph shape and time to peak.

For the recession analysis, only five individual storm hydrographs were used to calculate the baseflow and interflow parameters for the entire watershed. This might have caused the model to miss the baseflows and overestimate the peaks. Sujono et al. (2004) recommend using the correlation analysis and a larger sample of events for the recession coefficient calculation. Also, Fleming et al. (2004), Holberg (2015), and Singh et al. (2015) state the rainfall-runoff relationship shows variation for the different seasons, and thus seasonal or semi-annual parameterization may improve the model performance at the expense of increased parameter uncertainty.

Finally, the catchment was divided into fifteen sub-basins to better represent the climatic and hydrologic variability over the watershed area. This approach helped to average the basin characteristics on a local scale but led to increased model complexity during the calibration process. Since each sub-basin behaves uniquely during different hydrological events, it would be best to calibrate each sub-basin individually, but this was not possible due to the lack of gauge station at the outlet of each sub-basin. Thus, a single parameter (scaling) approach was used for the whole watershed (all 15 sub-basins).

This research can be extended to develop a fully distributed model by adding radar precipitation data and dividing the catchment into smaller grids. Results of this model could also be improved by using hourly rainfall, streamflow, and temperature data. Further, more accurate recession coefficients can be obtained by correlation analysis, which may improve the simulation results. Model performance could also be enhanced by extending the simulation period and using high-performance computing to run the automatic calibration algorithms available in HEC-HMS 4.2. Attempts to apply these automated methods in this study were not successful due to limited computational ability.

Finally, monthly and seasonal streamflow forecast analysis can be performed using statistical or dynamical climate forecasts as inputs to the model (Witham, 2015). Long-range projections of climate could also be combined with future land-use scenarios to apply the model in planning studies. It is hoped that use of the model can help the LCRA better understand the consequences of extreme hydrologic events and mitigate the effects of drought.

References

Ali, M., Khan, S. J., Aslam, I., & Khan, Z. (2011). Simulation of the impacts of land-use change on surface runoff of Lai Nullah Basin in Islamabad, Pakistan. *Landscape and Urban Planning, 102*(4), 271-279.

Allen, R. G., Pereira, L. S., Raes, D., & Smith, M. (1998). FAO Irrigation and drainage paper No. 56. *Rome: Food and Agriculture Organization of the United Nations, 56*(97), e156.

Arnold, J. G., Srinivasan, R., Muttiah, R. S., & Williams, J. R. (1998). Large area hydrologic modeling and assessment part I: model development. *JAWRA Journal of the American Water Resources Association, 34*(1), 73-89.

Bennett, T. H., & Peters, J. C. (2000). Continuous Soil Moisture Accounting in the Hydrologic Engineering Center Hydrologic Modeling System (HEC-HMS) *Building Partnerships* (pp. 1-10).

Beven, K. (2001). How far can we go in distributed hydrological modelling? *Hydrology and Earth System Sciences Discussions, 5*(1), 1-12.

Bhuiyan, H. A., McNairn, H., Powers, J., & Merzouki, A. (2017). Application of HEC-HMS in a Cold Region Watershed and Use of RADARSAT-2 Soil Moisture in Initializing the Model. *Hydrology, 4*(1), 9.

Bristow, K. L., & Campbell, G. S. (1984). On the relationship between incoming solar radiation and daily maximum and minimum temperature. *Agricultural and forest meteorology, 31*(2), 159-166.

CH2M, H. (2008). Climate change study: report on evaluation methods and climate scenarios. *Prepared for Lower Colorado River Authority and San Antonio Water System Water Project*.

Chow, V. T., Mays, L., & Maidment, D. R. (1988). *Applied hydrology*: Tata McGraw-Hill Education.

Clay, C., & Kleiner, D. J. (2017). Colorado River. *The handbook of Texas online*.

Cunderlik, J. (2003). *Hydrologic model selection for the CFCAS project: assessment of water resources risk and vulnerability to changing climatic conditions*: Department of Civil and Environmental Engineering, The University of Western Ontario.

Cydzik, K., & Hogue, T. S. (2009). Modeling Postfire Response and Recovery using the Hydrologic Engineering Center Hydrologic Modeling System (HEC-HMS). *JAWRA Journal of the American Water Resources Association, 45*(3), 702-714.

Devia, G. K., Ganasri, B., & Dwarakish, G. (2015). A review on hydrological models. *Aquatic Procedia, 4*, 1001-1007.

Dingman, S. L. (1994). *Physical hydrology*: Prentice Hall.

Fleming, M. (2002). *Continuous hydrologic modeling with HMS: parameter estimation and model calibration and validation.*

Fleming, M., & Neary, V. (2004). Continuous hydrologic modeling study with the hydrologic modeling system. *Journal of Hydrologic Engineering, 9*(3), 175-183.

Geethalakshmi, V., Kitterød, N., & Lakshmanan, A. (2008). *A literature review on modeling of hydrological processes and feedback mechanisms on climate*. Retrieved from

Ghaffari, G. (2011). The impact of DEM resolution on runoff and sediment modelling results. *Research Journal of Environmental Sciences, 5*(8), 691.

Gupta, H. V., Sorooshian, S., & Yapo, P. O. (1999). Status of automatic calibration for hydrologic models: Comparison with multilevel expert calibration. *Journal of Hydrologic Engineering, 4*(2), 135-143.

Gyawali, R., & Watkins, D. W. (2013). Continuous hydrologic modeling of snow-affected watersheds in the Great Lakes basin using HEC-HMS. *Journal of Hydrologic Engineering, 18*(1), 29-39.

Holberg, J. A. (2015). *Downward model development of the soil moisture accounting loss method in HEC-HMS: Revelations concerning the soil profile.* Purdue University.

Homer, C., Huang, C., Yang, L., Wylie, B., & Coan, M. (2004). Development of a 2001 national land-cover database for the United States. *Photogrammetric Engineering & Remote Sensing, 70*(7), 829-840.

Hutchinson, M. F., & Dowling, T. (1991). A continental hydrological assessment of a new grid-based digital elevation model of Australia. *Hydrological processes, 5*(1), 45-58.

Jain, S. K., & Singh, V. P. (2003). *Water resources systems planning and management* (Vol. 51): Elsevier.

Jajarmizadeh, M., Harun, S., & Salarpour, M. (2012). A review on theoretical consideration and types of models in hydrology. *Journal of Environmental Science and Technology, 5*(5), 249-261.

Kracman, D., McKinney, D., Watkins Jr, D., & Lasdon, L. (2006). Stochastic optimization of the highland lakes system in Texas. *Journal of Water Resources Planning and Management, 132*(2), 62-70.

LCRA. (2006). Colorado River Basin Watersheds. *MAPS.* Retrieved from http://maps.lcra.org/default.aspx?MapType=Watershed%20Posters

LCRA. (2015). Water Management Plan for the Lower Colorado River Basin. *Lower Colorado River Authority, Austin, TX*.

LCRA. (2017a-a). About LCRA. *Lower Colorado River Authority, Austin, TX.* Retrieved from https://www.lcra.org/about/Pages/default.aspx

LCRA. (2017a-b). Historic drought and the lower Colorado River basin. *MAPS.* Retrieved from www.lcra.org/water/water-supply/highland-lakes.../Fact-Sheet-General-Drought.

LCRA. (2017b). How the Highland Lakes work. Retrieved from https://www.lcra.org/water/floods/Pages/how-lcra-system-of-dams-works.aspx

LCRA. (2017d). Mansfield Dam and Lake Travis. Retrieved from https://www.lcra.org/water/dams-and-lakes/pages/mansfield-dam.aspx

Liang, X., Lettenmaier, D. P., Wood, E. F., & Burges, S. J. (1994). A simple hydrologically based model of land surface water and energy fluxes for general circulation models. *Journal of Geophysical Research: Atmospheres, 99*(D7), 14415-14428.

Linsley Jr, R. K., Kohler, M. A., & Paulhus, J. L. (1975). *Hydrology for engineers*: McGraw-Hill, Inc.

Lohmann, D., NOLTE-HOLUBE, R., & Raschke, E. (1996). A large-scale horizontal routing model to be coupled to land surface parametrization schemes. *Tellus A, 48*(5), 708-721.

McEnroe, B. (2010). Guidelines for continuous simulation of streamflow in Johnson County, Kansas, with HEC-HMS. *Department of Civil, Environmental and Architectural Engineering, Univ. of Kansas*.

Meenu, R., Rehana, S., & Mujumdar, P. (2013). Assessment of hydrologic impacts of climate change in Tunga–Bhadra river basin, India with HEC-HMS and SDSM. *Hydrological processes, 27*(11), 1572-1589.

Moriasi, D. N., Arnold, J. G., Van Liew, M. W., Bingner, R. L., Harmel, R. D., & Veith, T. L. (2007). Model evaluation guidelines for systematic quantification of accuracy in watershed simulations. *Transactions of the ASABE, 50*(3), 885-900.

Nash, J. E., & Sutcliffe, J. V. (1970). River flow forecasting through conceptual models part I—A discussion of principles. *Journal of Hydrology, 10*(3), 282-290.

Ponce Victor, M. (1989). Engineering Hydrology, Principles and Practices: Prentice Hall, Englewood Cliffs, New Jersey, USA.

Ryu, J. H., Sohrabi, M., & Acharya, A. (2014). Toward mapping gridded drought indices to evaluate local drought in a rapidly changing global environment. *Water resources management, 28*(11), 3859-3869.

Shaw, E. M., Beven, K. J., Chappell, N. A., & Lamb, R. (2010). *Hydrology in practice*: CRC Press.

Shellito, B. A. (2011). *Introduction to geospatial technologies*: Macmillan Higher Education.

Singh, W. R., & Jain, M. K. (2015). Continuous Hydrological Modeling using Soil Moisture Accounting Algorithm in Vamsadhara River Basin, India. *J. Water Res. Hydraul. Eng, 4*, 398-408.

SSURGO. (1995). *Soil Survey Geographic (SSURGO) Data Base: Data Use Information*: National Cartography and GIS Center.

Sujono, J., Shikasho, S., & Hiramatsu, K. (2004). A comparison of techniques for hydrograph recession analysis. *Hydrological processes, 18*(3), 403-413.

Tramblay, Y., Bouvier, C., Martin, C., Didon-Lescot, J.-F., Todorovik, D., & Domergue, J.-M. (2010). Assessment of initial soil moisture conditions for event-based rainfall–runoff modelling. *Journal of Hydrology, 387*(3), 176-187.

University of Washington. (2015, 2015). *VIC Calibration.* Retrieved from http://vic.readthedocs.org/en/master/Documentation/Calibration

USACE. (2000). *HEC-HMS Hydrologic Modeling System-Technical Reference Manual*. Retrieved from

USACE. (2016). HEC-HMS Hydrologic Modeling System- User Manual. *US Army Corps of Engineers-Hydrologic Engineering Center. USA*.

Verma, A. K., Jha, M. K., & Mahana, R. K. (2010). Evaluation of HEC-HMS and WEPP for simulating watershed runoff using remote sensing and geographical information system. *Paddy and Water Environment, 8*(2), 131-144.

Watkins, D. W., McKinney, D. C., Lasdon, L. S., Nielsen, S. S., & Martin, Q. W. (2000). A scenario-based stochastic programming model for water supplies from the highland lakes. *International Transactions in Operational Research, 7*(3), 211-230.

Wei, W., & Watkins, D. W. (2011). Probabilistic streamflow forecasts based on hydrologic persistence and large-scale climate signals in central Texas. *Journal of Hydroinformatics, 13*(4), 760-774.

Williams, J., & William, M. (2017). Colorado River. *The handbook of Texas online*.

Witham, J. D. (2015). *Calibration, verification, and diagnosis of a season-ahead drought prediction model: Limits to predictability in central Texas.* Michigan Technological University.

Xu, C.-y. (2002). Hydrologic models. *Textbooks of Uppsala University. Department of Earth Sciences Hydrology*.

Zelenhasić, E., & Salvai, A. (1987). A method of streamflow drought analysis. *Water resources research, 23*(1), 156-168.

Zhang, W., & Montgomery, D. R. (1994). Digital elevation model grid size, landscape representation, and hydrologic simulations. *Water resources research, 30*(4), 1019-1028.

Zimmerman, B. G., Vimont, D. J., & Block, P. J. (2016). Utilizing the state of ENSO as a means for season-ahead predictor selection. *Water resources research, 52*(5), 3761-3774.

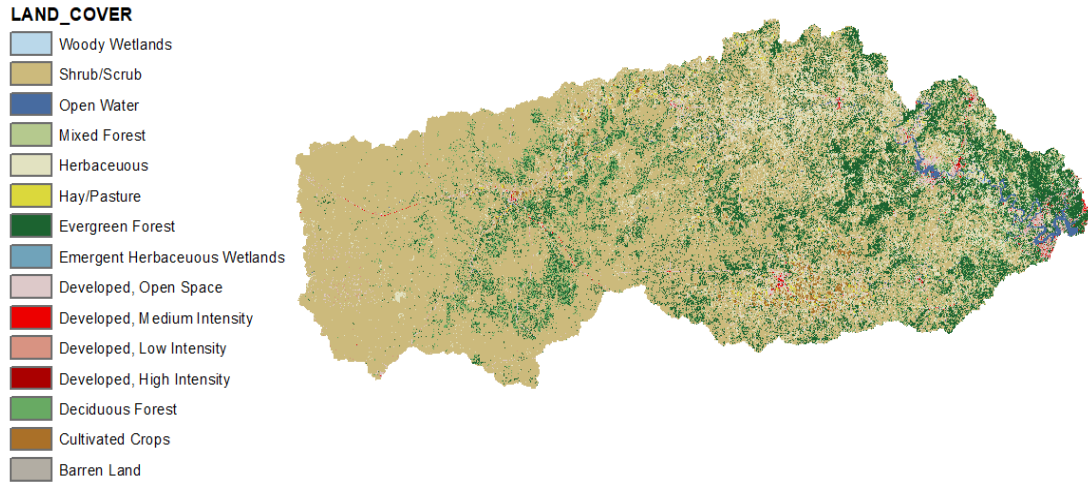# Appendix A. Raster of SMA parameters

Land cover raster

Figure 23: Land cover raster (Source NLCD)
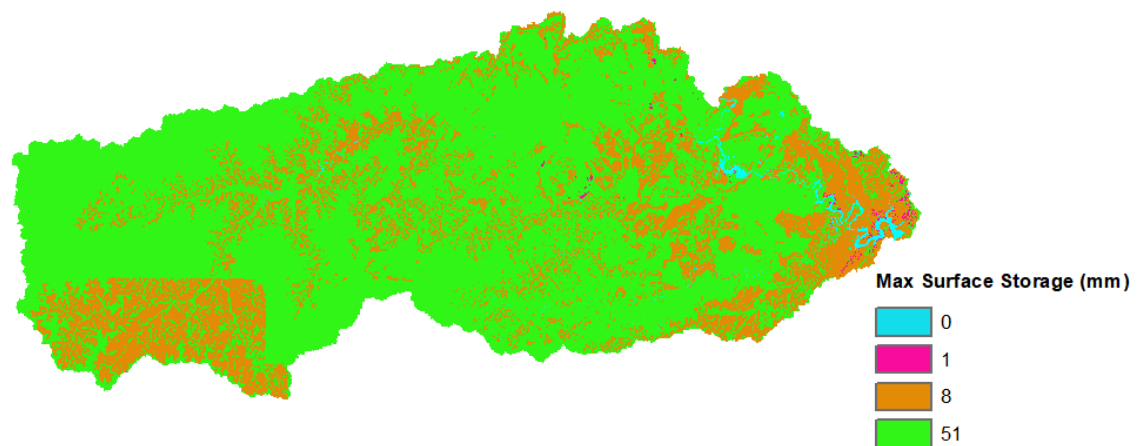
Surface storage raster

Figure 24: Surface storage raster based on SSURGO database
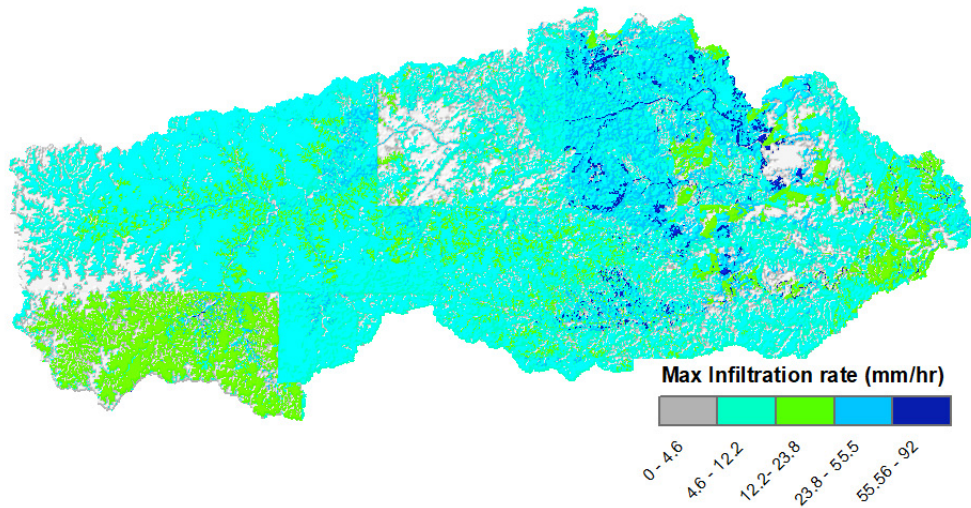
Maximum infiltration rate raster

Figure 25: Maximum infiltration rate based on SSURGO database

Maximum soil storage raster
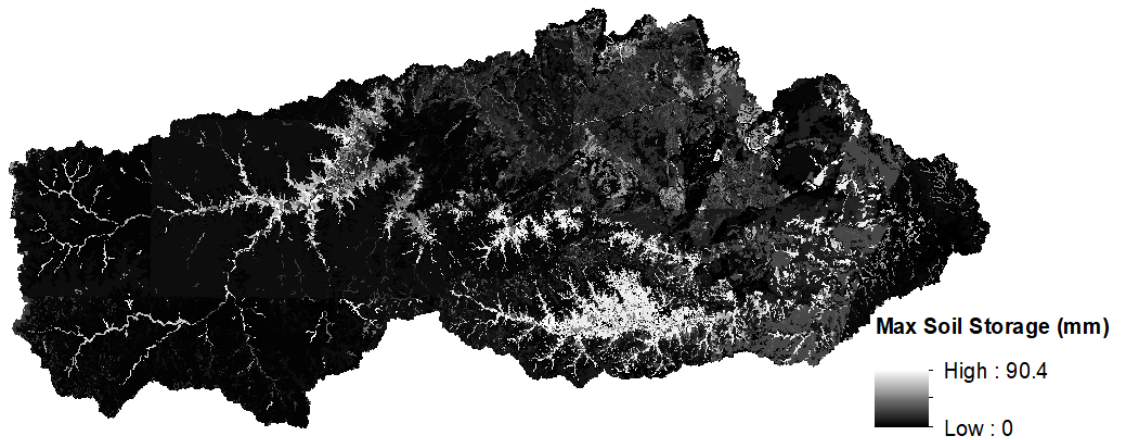
Figure 26: Maximum soil storage raster based on SSURGO database

Appendix B. Stream Recession Analysis

Table 11: Recession analysis results

Llano River	2014	2015	2016	2016₂	2016₃	Max/Ave	(Hour)
	10	6	3	9	11		
Baseflow storage (mm)	2.44	5.29	6.8	7.5	7	**7.50**	
Baseflow Recession Constant	79.00	9.09	26.31	47	55	**43.28**	1038.74
Interflow Storage (mm)	0.12	1.35	0.5	1.7	0.44	**1.70**	
Interflow Recession Constant	2.58	1.15	2.85	1.96	2.34	**2.18**	52.21

Appendix C. Basin Summary

Project: trail&errocopy   Simulation Run: Run 146

Start of Run: 01Jan2004, 00:01   Basin Model: travislbj
End of Run: 31Dec2011, 00:01   Meteorologic Model: travislbj
Compute Time:DATA CHANGED, RECOMPUTE   Control Specifications:Calibration

Show Elements: All Elements   Volume Units: ○ MM ● 1000 M3   Sorting: Hydrologic

Hydrologic Element	Drainage Area (KM2)	Peak Discharge (M3/S)	Time of Peak	Volume (1000 M3)
W720	1013.3	203.2	27Jun2007, 23:01	309141.1
W710	1177.0	229.2	17Nov2004, 11:01	394031.2
W920	2186.0	2398.2	16Aug2007, 10:01	1442997.3
W900	624.68	613.9	27Jun2007, 01:01	428286.4
W660	565.08	404.9	17Aug2007, 04:01	177164.3
W830	1460.8	100.6	17Aug2007, 08:01	187064.3
W1020	1127.0	460.3	12Sep2009, 07:01	157230.3
W610	1192.0	14.7	23Aug2007, 12:01	94768.6
W600	1722.4	324.1	28Jun2007, 08:01	580094.1
W820	957.79	11.9	26Aug2004, 07:01	98223.3
W580	1172.5	314.7	17Aug2007, 07:01	326336.7
W790	995.85	989.7	12Sep2009, 02:01	272444.8
W1000	1281.5	18.6	16Sep2009, 12:01	144296.9
W520	1048.1	29.5	27Oct2009, 19:01	262743.0
W940	1126.3	634.8	22Oct2009, 08:01	432749.8
Outlet1	17650.30	2231.4	17Aug2007, 00:01	5308385.0

Figure 27: Calibration global summary

Project: trail&errocopy   Simulation Run: Run 147

Start of Run: 01Jan2012, 00:00   Basin Model: travislbj
End of Run: 31Dec2016, 00:00   Meteorologic Model: travislbj
Compute Time:DATA CHANGED, RECOMPUTE   Control Specifications:Validation

Show Elements: All Elements   Volume Units: ● MM ○ 1000 M3   Sorting: Hydrologic

Hydrologic Element	Drainage Area (KM2)	Peak Discharge (M3/S)	Time of Peak	Volume (MM)
W720	1013.30	160.8	29May2015, 08:00	99.27
W710	1177.00	250.0	29May2015, 07:00	156.94
W920	2186.00	40.4	01Jun2016, 22:00	247.13
W900	624.68	424.0	30Oct2015, 05:00	484.88
W660	565.08	8.5	31May2015, 04:00	74.41
W830	1460.80	179.0	29May2015, 07:00	54.82
W1020	1127.00	16.3	31May2015, 20:00	46.81
W610	1192.00	16.5	28May2015, 02:00	44.37
W600	1722.40	37.3	28May2015, 20:00	119.62
W820	957.79	9.7	30May2015, 04:00	41.01
W580	1172.50	162.0	29May2015, 06:00	71.78
W790	995.85	480.8	24May2015, 02:00	78.80
W1000	1281.50	17.4	29May2015, 01:00	50.10
W520	1048.10	25.3	29May2015, 11:00	113.14
W940	1126.30	599.9	26May2015, 04:00	179.31
Outlet1	17650.30	1114.4	26May2015, 11:00	121.79

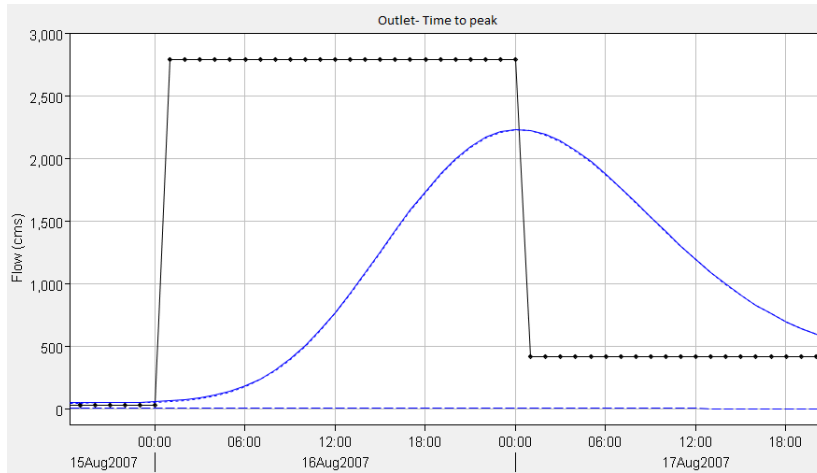*Figure 28: Validation global summary*

Appendix D. Time of Peak Results

Figure 29: Example results for Time of Peak